Teleoperation Platform for Micromanipulation and Characterization of Single Cells

A Thesis

Submitted to the Faculty

of

Drexel University

by

Umut Yesilmen

in partial fulfillment of the

requirements for the degree

of

Master of Science

In

Biomedical Engineering

July 2005

Drexel University
Office of Research and Graduate Studies
Thesis Approval Form
(For Masters and Doctoral Students)

Hagerty Library will bond a copy of this form with each copy of your thesis/dissertation.

This thesis, entitled Teleoperation Platform for Micromanipulation and Characterization of Single Cells

and authored by Umut Yesilmen, is hereby accepted and approved.

Signatures:

Chairman, Examining Committee: _____

Supervising Professor: R. Sellar

Committee Members: _____ _____

_____ _____

_____ _____

Program Advisor: _____

Department Head: R. Sellar

Dedications

To my mother and father for their love, support, effort, and patience.

Acknowledgements

I feel very special to have the opportunity to work with two greatest advisors; Dr. Rahamim Seliktar and Dr. Vijay Kumar. I wish every student could have such advisors.

Dr. Kumar accepted me to the GRASP Lab at UPenn as a visiting graduate student at the time when I was very hopeless to find a research that fits my background. I would like to thank him for his kindness all the time, giving me time always even he had a hectic schedule, and great advising. I would like to thank Dr. Seliktar for his patience on me, supervising, encouraging me all the time, listening and understanding me, being very kind, and his coffee offers. My very special thanks to Dr. Bahrad Sokhansanj for his support and selecting me as his teaching assistant. It was my honor to work with him. I would like to thank Dr. Kenneth A. Barbee for being in my committee.

Thanks to all GRASP Lab people. Very special thanks go to Dr. Peng Song for his continuous help and support at the beginning and later parts of the project. He was a great tutor to me. I would like to thank David Cappelleri, my project partner, for his friendship, help, reviewing my thesis, and encouragement. Thank you very much Katerina Canakis and Tara Betterbid; for your kindness and helping me in administrative work. Terry Kientz's help in instrumentation and

technical problems was invaluable. I would like to thank also to PRISM Lab faculty and students, especially Dr. Jaydev Desai and Anand Pillarisetti for answering our questions very kindly all the time.

I would like to thank my best lab partner Hakan Yazarel, the lab and weekday life could be very boring without him. His encouragement and help in some of the mathematical subjects were invaluable.

And we come to the weekends; very special thanks go to M. Fatih Akay. Thank you for all the friendship. We had a lot of fun, learned a lot, and refreshed our minds while we did what we did. I am waiting for the time when we will tell the "son söz" with other friends Fuat, Mete, Kemal in Kıbrıs.

Şafak, thank you for your love. Without you, nothing would have a meaning in my life.

I can never express how much I am thankful to my mother and father.

Table of Contents

List of Tables

List of Figures

Abstract

Teleoperation Platform for Micromanipulation and Characterization of Single Cells

Umut Yesilmen
Vijay Kumar, Ph.D.
Rahamim Seliktar, Ph.D.

A teleoperation platform for micromanipulation and characterization of single cells has been developed. The platform has the local site and the remote site. The operator at the local site controls the micromanipulator via PHANToM force feedback device by feeling the force applied to the cell and viewing the manipulation environment. The remote site has the following components: Two micromanipulators for holding and manipulating the cell, the force sensor with a resolution of 50 μN, microscope, camera, and the cell. Five sets of experiments are performed to demonstrate the performance of the teleoperation platform. White fish egg cells with an average diameter of 2000 μm are used in the cell experiments. The experimental data are used to analyze the viscoelastic properties of the egg cell as well as the factors affecting the stiffness of the cell such as osmosis, diameter, and salinity level.

1. Introduction

Teleoperation is the field where an operator's manipulation capability and sensing are extended to another location (i.e. remote site) in order to operate a machine away from the operator. Teleoperation is used in many different areas such as space technology, undersea research, nuclear power reactors, toxic waste cleaning, construction, agriculture, mining, warehousing and mail delivery, firefighting and lifesaving, policing, military operations, assistive devices for the disabled, telediagnosis, telesurgery, and entertainment. [Sheridan, 1992]

In order to control the machine from another location, the operator needs feedback. The increase in information flow between the sites will increase the operator's performance. In a teleoperated needle insertion study, Gerovichev, et al. (2002) showed that force feedback reduced error in detection of transitions between tissue layers by at least 55%, the addition of visual feedback improved the operator's performance by at least 87%, where as the addition of both visual and force feedback improved performance by at least 43% in comparison to scenarios without feedback.

The two important feedback elements of the teleoperation are visual and force feedback. In most of the teleoperation systems visual display is supplied to the operator. Visual feedback requires almost no computation unless a virtual

environment is rendered and displayed. Coupling force feedback with vision brings challenges as well as trade-offs. As an example; the update rate of the force feedback must be at least 500 Hz, where as 16 Hz is required for visual feedback. Thus, they must run asynchronously in the system which brings computational and communicational challenges. Another example can be that the higher visual quality will cause delays in the network, and reduce the feedback rate, so that a local model of the remote site material is included in some systems to predict the force applied. And also if the force feedback frequency is less than required, it causes unpleasant vibrations, and stiff surfaces become softer or unstable [Adachi et al., 1995].

Micromanipulation is an application of teleoperation where the operator's manipulation and sensing capabilities are carried to a micro-scale environment. Micromanipulation brings its own challenges over teleoperation. Unlike macro world, gravity is negligible in micro world, but on the other hand attractive forces (i.e. Van der Waals, electrostatic, and surface tension forces) are dominant. [Arai et al., 1995] As an example, in this research project, it is experimented that picking up microspheres with a pipette is easier than releasing, since microspheres tend to stick on the pipette. Microspheres could only be removed from pipette by blowing air or shaking the pipette every time.

In micromanipulation, supplying the operator with visual feedback is easier compared to force feedback, since there are many commercial microscopes are

available in the market. Addition of a force feedback capability in micromanipulation system can be based on physical contact or vision based force sensors. An overview about the works on these two approaches by different research groups will be made in the next section.

In this thesis, a tele-micromanipulation platform for manipulating single cell organisms with force feedback based on a load cell force sensor is presented. The goal of this platform is to be able to manipulate objects in the range of hundreds to thousands micrometers. The force sensor used should be able to supply the operator with a satisfactory force feedback so that the change in the smallest force change will not be felt discretely (i.e. the resolution of the force sensor should be high enough to give a smooth change in the force). Also, the general requirements for a teleoperation platform must be satisfied which are minimum of 500 Hz force and 16 Hz visual feedback at the local site.

The platform consists of two sites; local and remote site. Figure 1 shows our tele-micromanipulation platform architecture. The operator sits on the local site, whereas the material to be manipulated is on the remote site. Visual feedback, force feedback, and motion control commands between the two sites are communicated and carried by a two-way network.

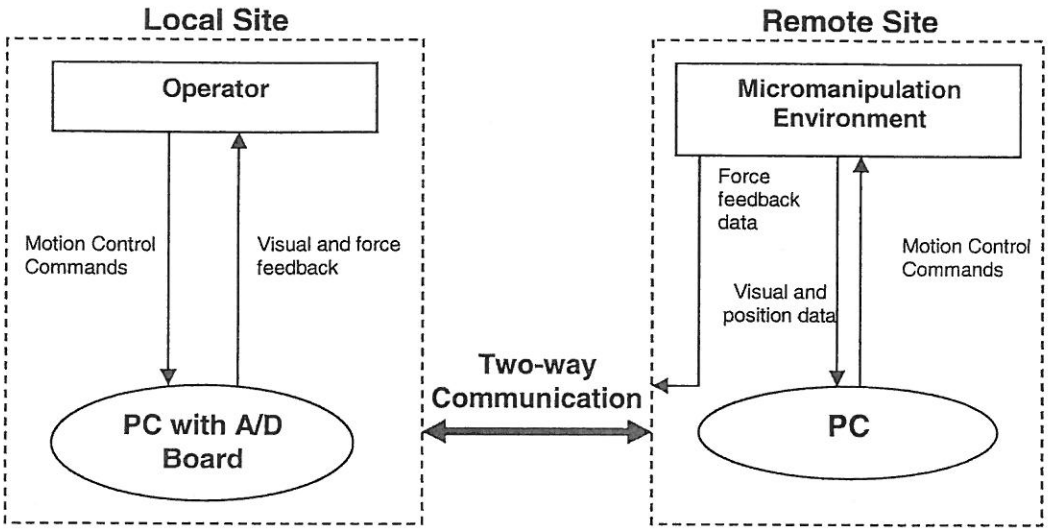

Figure 1 - Tele-micromanipulation Platform Architecture

The local site system setup consists of one force feedback device (PHANToM Premium 1.5 of SensAble Technologies, Inc.), and one personal computer, as seen in Figure 2. The remote site system setup consists of one inverted optical microscope (TE2000-U of Nikon, Inc.), one CCD Camera (XC-77 of Sony, Inc.), load cell (GSO-10 load cell of Transducer Technologies, Inc) as the force sensor, two micromanipulators (Model MX7600R of Siskiyou Design Instruments, Inc. and Two-axis 5-inch Square Linear Translation Stage of Edmund Optics, Inc.), and one personal computer, as seen in Figure 3.

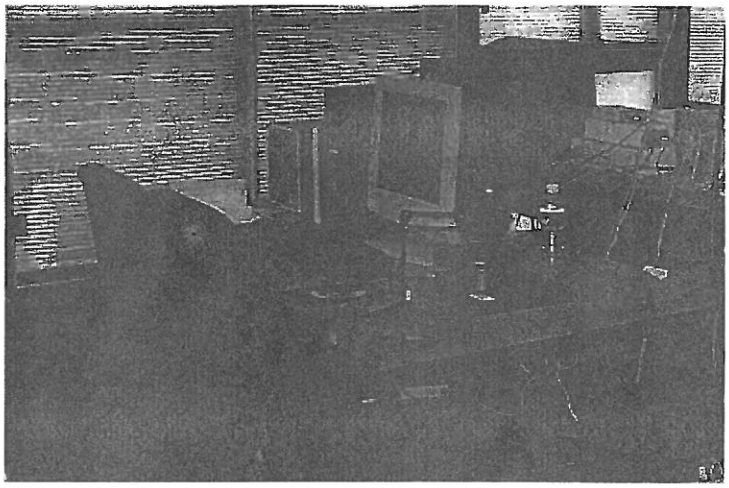

Figure 2 - Teleoperation platform - local site

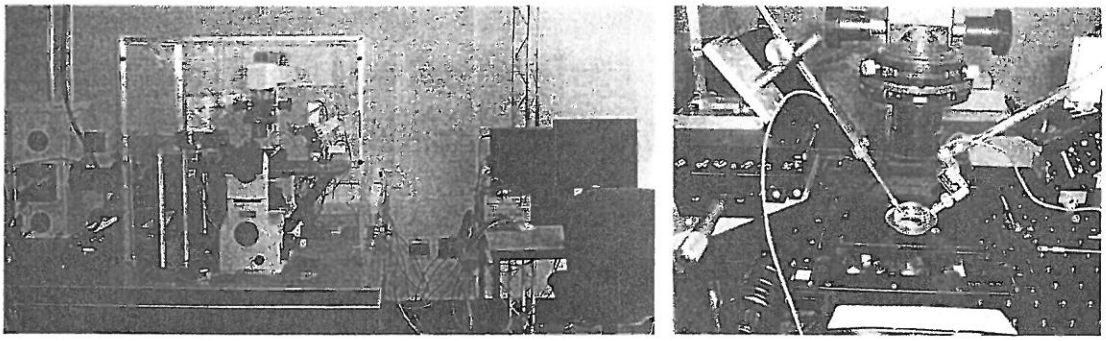

Figure 3 - Teleoperation platform - remote site

The image of the material under the microscope (e.g. cell and extracellular matrix) is captured by CCD camera as a bitmap image; it's then compressed to JPEG image file, and sent to the local site over internet. The received image is displayed on the operator's screen. Update rate of the image frames in both remote and local sites is 30 Hz.

The force applied to the material under the microscope is calculated by using a strain gauge based load cell. The force applied to the material creates a linear voltage at the load cell. And the voltage value is digitized by an A/D Board, retrieved by the local site software, and finally the force value corresponding to the digitized voltage is calculated by predefined calibration equation which will then be applied to the operator by PHANToM force feedback device. In the current system, the output of the A/D Board is directly connected to the computer at local site, and the output rate is 330 kHz.

The motion control commands are sent from local site to the remote site over a network. The operator uses the PHANToM's arm as a control device. The two-dimensional position vector of PHANToM tip is transformed in the micromanipulator reference frame coordinates, and then sent to the remote site. These transformed coordinates are then sent from the PC to the micromanipulator via serial stream port. The pipette position is also acquired from micromanipulator, and then sent to the local site. The third dimension (z-axis) is ignored, since the system works in two-dimensional space. Update rate for motion control commands is 30 Hz.

In order to demonstrate the performance of the platform satisfying the requirements stated above, five different sets of experiments are implemented. The overall performance of the teleoperation platform is tested by a microassembly experiment, namely peg-in-the-hole problem, where the operator

controls the micromanipulator to push an object along a groove to its target position by translation and rotation. It is shown that the operation takes 64 seconds.

The following three experiments are implemented to to observe the force sensor and micromanipulator capabilities as well as the characteristics of the cell being used with the collected data. White fish egg cells with a diameter around 2000 μm are used in the experiments. One of the micromanipulators having a micro needle and force sensor is moved with certain indentation levels to push the cell membrane while the other micromanipulator having the suction device holds the cell in position. The force measurements are collected and used afterwards to analyze the viscoelastic properties of the cell, the time dependency of stiffness during osmosis of the cell, and the cellular force is dependency on diameter. Also the salinity level effects on the egg cell are tested and analyzed.

The last experiment is designed to see if the force feedback is useful and increases the time efficiency of the platform. The operator tried to complete the given task in manual mode without force feedback and teleoperation mode with force feedback. The time to complete the operation is recorded in both cases and then compared to see whether there is efficiency or not by using force feedback.

2. Existing Knowledge

Using micromanipulation techniques such as holding, moving, injecting/ejecting materials in/out the cell can be called as "biomanipulation". Biomanipulation is an important field for the characterization and manipulation of single embryo cells in applications such as cloning, gene expression analysis, and cell replacement therapy (CRT). These techniques take place in agricultural industry, individual-cell-based diagnosis, and pharmaceutical testing. [Park et al., 2005]

Two most common areas where biomanipulation have been used are intracytoplasmic sperm injection (ICSI) and embryo pronuclei DNA injection. ICSI operators are required to have at least one year full-time training, and the success rate is very low; according to Kapoor et al. (2003), the success rate has a marginal 40% - 70% survival rates for only cell microinjection, where as the success rate for the entire transgenic task is 1%-4%. It's shown that autonomous cell injection techniques improve the success rate up to 100% by different research groups, which will be discussed in the next section.

Automated biomanipulation systems can be classified as contact manipulation, which is mechanical micromanipulation, and non-contact biomanipulation can be subdivided further as electro-rotation and laser trapping [Sun et al 2001].

The electro-rotation technique is based on controlling the phase shift and magnitude of electric fields. Using electric fields, torque is applied to the cell for positioning [Sun et al 2001]. Park et al (2005) developed an integrated cell processor for the automatic handling of individual embryo cells, which can perform functions such as cell transport, isolation, orientation, and immobilization. Their system is an example of non-contact biomanipulation with electro-rotation techniques. They use microfluidic and PPy valves to minimize manual handling steps and fluid flow by an external pressure to transport embryos in the micro-channel. Embryo cells are placed in a reservoir on the microfluidic device. The cells are then moved through the channels to an injection port by pressure driven fluid flow. During the flow, the operator can see the embryo cells under the microscope, and as soon as the target cell passes the PPy valves, the operator closes the PPy valves to isolate the target cell and prevent other embryo cells from passing. Cell immobilization and moving to the injection port is achieved by the suction from a micro-hole. The target cell orientation - which is essential for high fertilization - is automated by electro-rotation technique for optimal angle of the cell injection site. [Park et al 2005] Their cell processor system can be seen in Figure 4.

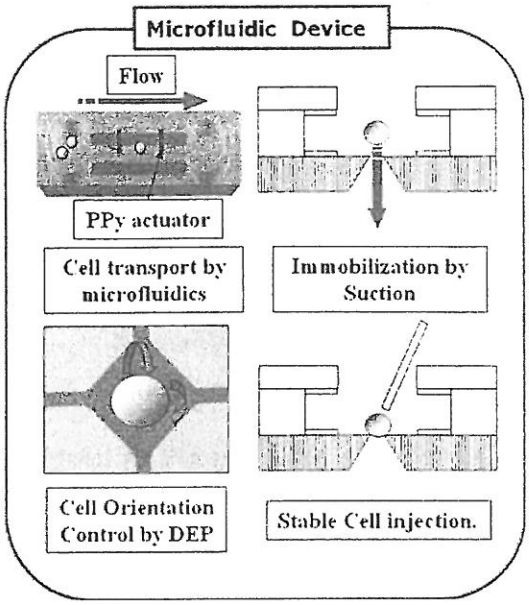

Figure 4 - The cell processor (Park et al, 2005)

In the laser trapping technique, a laser beam is focused through a numerical aperture microscope objective which forms an optical trap at the focus. With the optical trap formed, the cell is pulled and trapped at the focus. There are several works on this technique by Ashkin et al (1970), Bruican et al (1987), Conia et al (1997), and Wright et al (1990). One of the disadvantages of laser trapping technique is that high energy light close to UV spectrum is applied to the aqueous solution which can be harmful to the cell. The other disadvantage is that the incident laser beam light can cause genetic abnormalities on the cell. [Sun et al 2001]

The lack of a holding mechanism and possible damage to the cell is tried to be solved by using contact manipulation techniques. In this technique, there is a physical holding mechanism and a moving manipulation end for the operation. Kimura et al (1995) developed a piezo-driven micropipette for ICSI in the mouse. Their system has two ends for holding and injection. On the holding end, they use a holding pipette which is attached at the end of a suction device for holding the oocyte to be manipulated. At the injection end, they have a piezo-driven micropipette which does the injection for ICSI. They showed that using a piezo-driven micropipette is more effective than using the conventional pipette. The piezo-driven pipette can break the oolemma consistently. Their results show that only 16% of the oocytes survived under conventional sperm injection method, where as the survival rate is 80% under their piezo-driven method. [Kimura et al 1995] Figure 5 shows the two ends of their system. The arrow indicates the sperm injected.

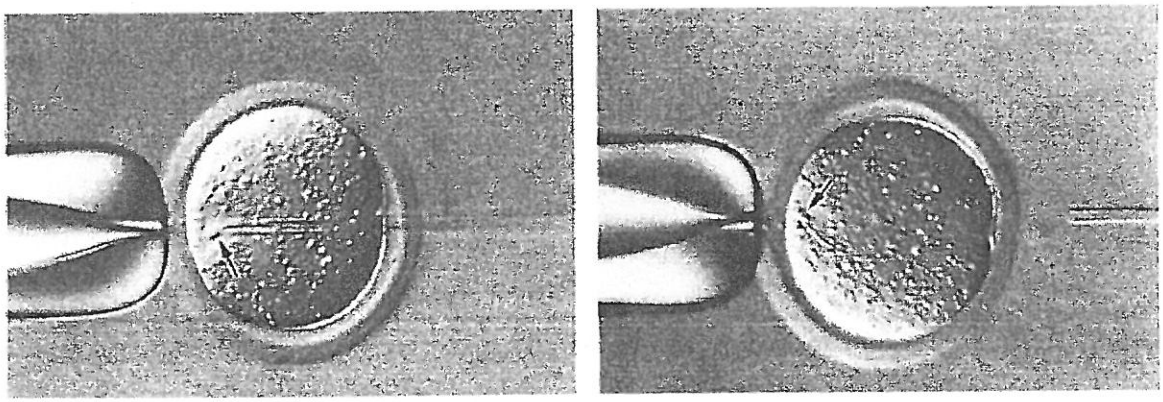

Figure 5 - Piezo-driven micropipette (Kimura et al, 1995)

As another approach, Tanikawa et al (1999) developed a micromanipulation system for assembling micro-machines, manipulation of biological cells, and performing micro-surgery. They used parallel mechanisms to develop a micro-hand having two fingers. The forefinger and thumb are used to control two end-effectors for manipulation. They were able to pick up and position a microscopic glass ball with a 2 μm diameter. The positioning accuracy was less than 0.1 μm. [Tanikawa et al 1999]

Figure 6 shows the configuration of the experimental system setup on the left, and the operational device on the right. They have no force feedback in this system.

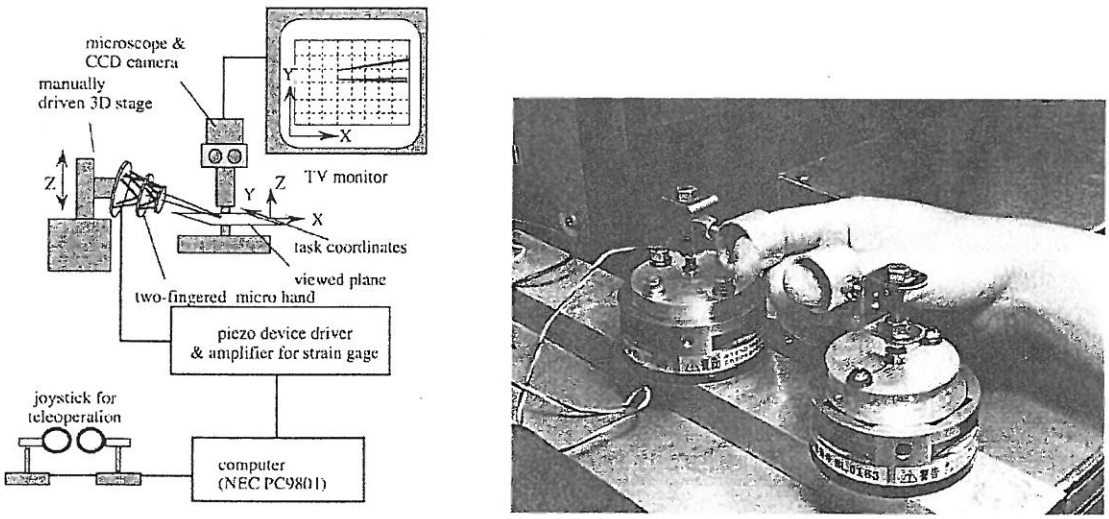

Figure 6 - Two fingered micro-hand system setup (left), operational device (right) (Tanikawa et al, 1999)

Ando et al (2001) proposed a tele-micromanipulation system with haptic feedback and a parallel micromanipulator (Figure 7). They used a parallel mechanism for the micromanipulator to improve accuracy and stiffness. They haven't showed the use of their system in cell manipulation.

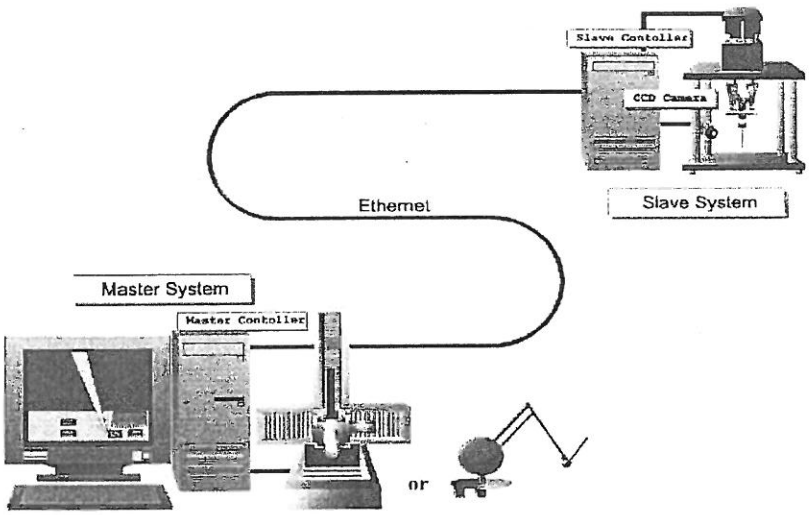

Figure 7 - Micro-teleoperation system architecture (Ando et al, 2001)

Sun et al (2003) developed a microelectromechanical systems-based multiaxis cellular force sensor for characterization of mouse zona pellucida and to analyze the mechanical property differences of zona pellucida before and after fertilization. The MEMS-based force sensor has dimensions of 3.2 mm and 3 mm in x and y directions, respectively. It can measure forces up to 25 μN with a resolution of 0.01 μN. They constructed an analytical biomembrane elastic model

to describe membrane properties. They showed that the characterized elastic modulus of embryos is 2.3 times greater than oocytes and the puncturing force of embryos is 1.7 times greater than oocytes.

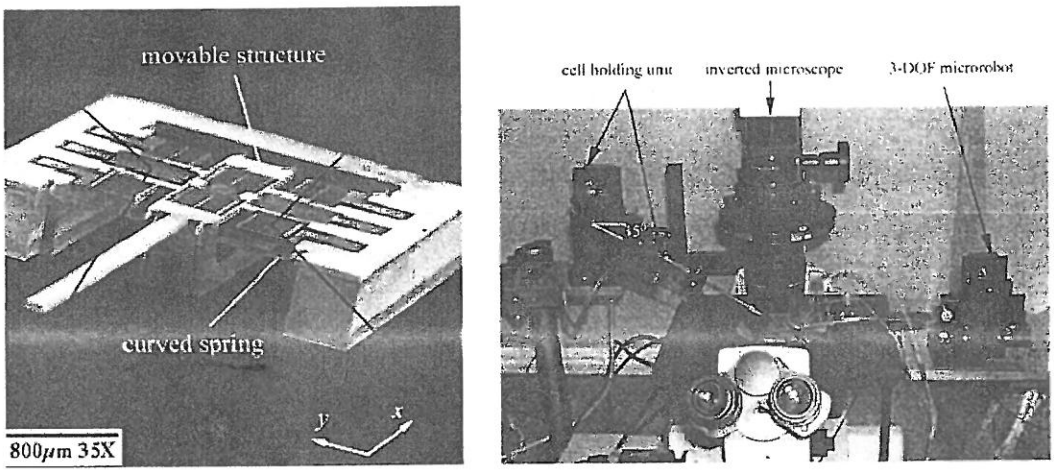

Figure 8 - Force sensor (left) and biomanipulation system setup (right) (Sun et al, 2003)

From the experimental observation, they proposed a biomembrane point-load model where the membrane shape can be characterized with three geometric parameters; a, w_d, and R, which are the dimple radius, dimple depth, and radius of the semicircular curved surface, respectively (Figure 9).

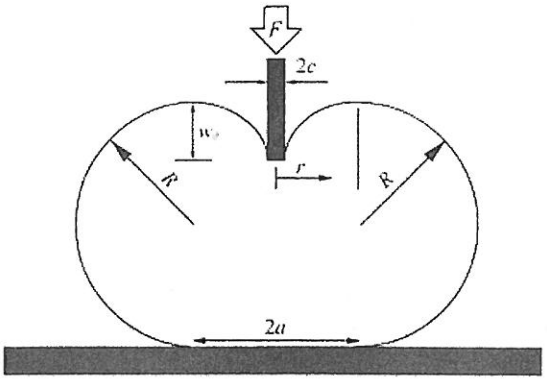

Figure 9 - Indentation of a cell membrane by a micropipette (Sun et al, 2003)

Davidson et al (1999) measured the composite elastic modulus of the cellular and extracellular matrix layers in the blastula wall of Strongylocentrotus purpuratus embryos at the mesenchyme blastula stage. These two layers exhibited a viscoelastic response with an initial stiffness ranging from 600 Pa to 2300 Pa. They used compression tests in a chamber sandwiched between two pieces of glass coverslip with silicone grease. They used calibrated mica-tipped needles to compress the embryo, and they measured the force by the deflection of the needle. By recording the compression test, they were also able to measure specific parameters such as the mica sheet displacement d, initial radius R_0, radius of the contact area R_c, the circumferential radius of the embryo R_1, and the meridian radius of the embryo R_2 as seen in Figure 10. These parameters were then used to calculate the elastic modulus of the wall tissue of the compressed mesenchyme blastula. To model the tissue's viscoelastic behavior, they used the standard linear model, also presented in Figure 10. As a result, they found that

the decrease in stiffness during the compression test indicated that the sea urchin's blastula wall acted as a viscoelastic material.

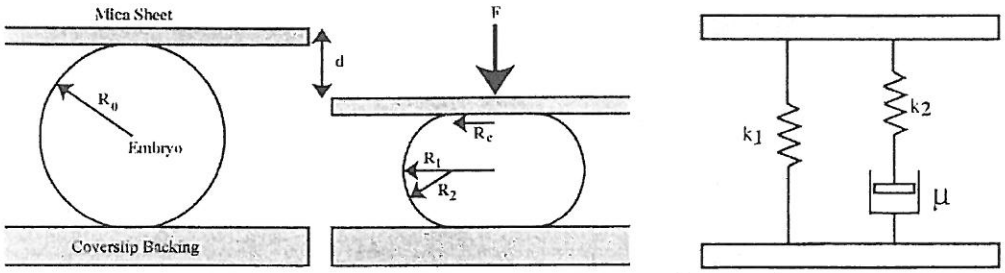

Figure 10 - The compression test of a S. purpuratus embryo at the mesenchyme blastula stage (left), standard linear model for viscoelastic response respresentation (right) (Davidson et al, 1999)

Pillarisetti et al (2005) developed a force feedback interface having a capability of measuring forces in the range of μN to mN. They used one-dimensional PVDF piezoelectric polymer film as the real time force sensor. Cell puncturing experiments are done on salmon and flying fish egg cells which have 7mm and 1mm of diameter, respectively. They were able to show that the cell puncturing forces were consistent and the operator was able to feel the cell injection forces. The puncturing forces were measured as 1.69 mN and 2.38 mN for the flying and salmon fish egg cells, respectively.

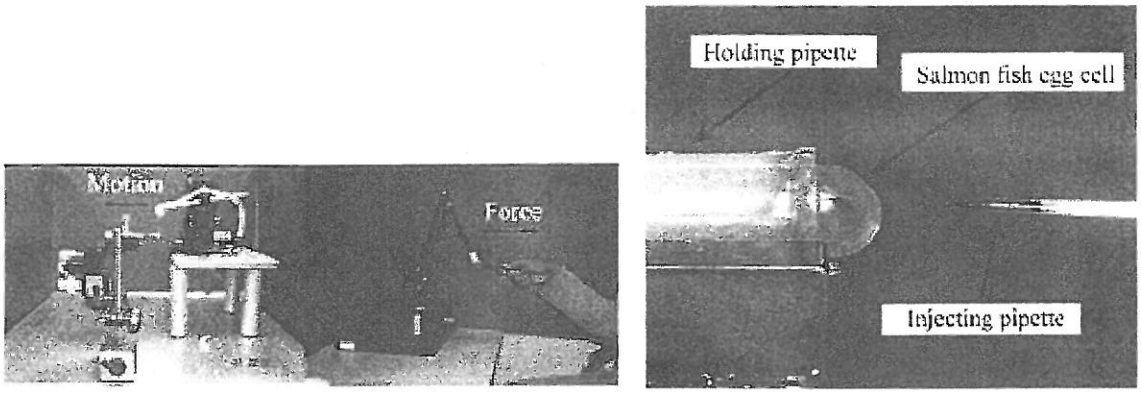

Figure 11 - The micromanipulation and force feedback environments (left), the injection of salmon fish egg cell (right) (Pillarisetti et al, 2005)

3. Materials and Methods

3.1 PHANToM Force Feedback Device

In this project, the PHANToM® Premium 1.0 of SensAble Technologies, Inc. is used as the force feedback and manipulator controller device. The PHANToM provides 3 degrees of freedom in position and force feedback (x, y, and z axes). An encoder can be mounted at the stylus in order to have 3 degrees of positional sensing which are pitch, yaw, and roll. It has a workspace of 13 x 18 x 25 cm, nominal position resolution of 0.03 mm, maximum exertable force of 8.5 N, 24 hours continuous exertable force of 1.4 N, stiffness of 3.5 N/mm, and footprint of 25 x 33 cm. The PHANToM device connects to the PC via the parallel port (EPP) interface. [PHANToM Product Catalog]

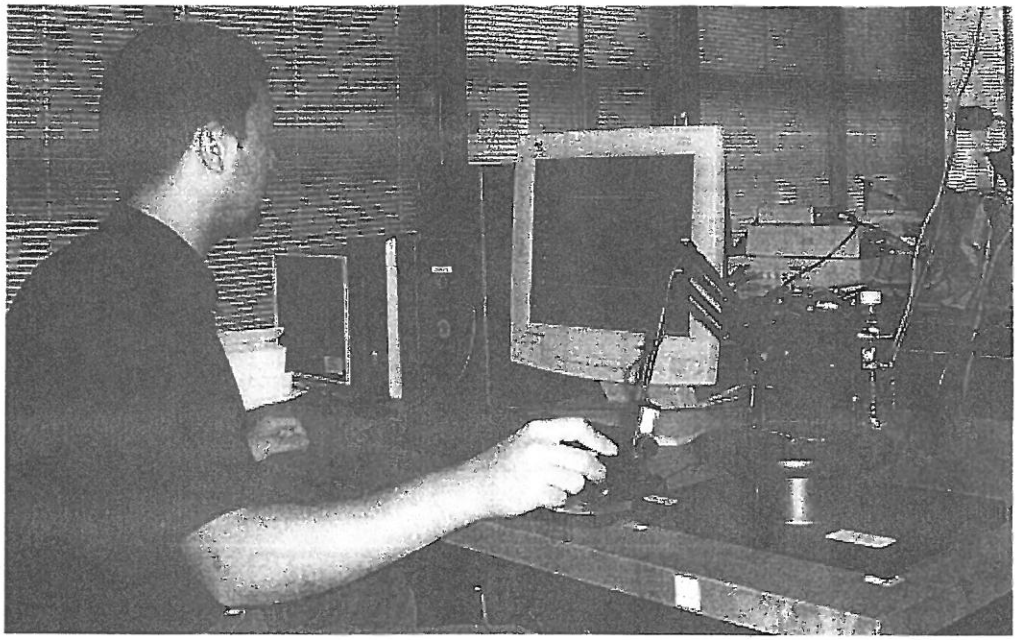

Figure 12 - PHANToM Premium 1.0 of SensAble Technologies, Inc.

The PHANToM device has General Haptics Open Software Toolkit (GHOST SDK) which is a C++ object oriented toolkit that can be used to represent the haptic environment and interact with the virtual objects specified in the scene. By using GHOST SDK, the programmer does not need to be concerned with low-level force and device issues. The objects in the environment can be defined in a hierarchical collection of nodes by using GHOST SDK. OpenGL based classes can be used in order to display a visual representation of the environment. A typical application consists of two processes; one process for handling the force feedback process (the servo control loop) and another process for handling specific application (core) functions such as graphics. The flow of this application can be graphed as in Figure 13.

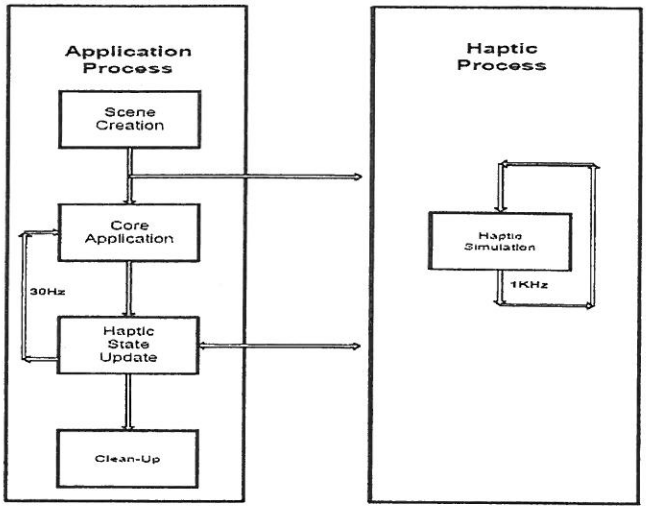

Figure 13 - Flow of a typical haptic application (GHOST SDK Programmer's Guide)

To meet the purposes of this project, gstDeviceIO class is used which gives the ability to directly access the encoders and motors of the PHANToM. With this class, the encoder values can be filtered, and forces can be directly sent to the motors. By taking advantage of low-level control on the force feedback device with gstDeviceIO class, the gravity compensation, cellular forces and any other forces can be combined and sent to the device and thus to the operator [GHOST SDK Programmer's Guide].

3.1.1 Gravity Compensation

When the PHANToM device is released freely on the air, the stylus tends to fall down because if the device's mass. This mass causes the operator feel the force coming from the device's own weight all the time. In order to cancel this force effect, gravity compensation is necessary, so that the operator will only feel forces generated by the application functions such as cellular force.

The diagram for PHANToM device workspace is shown below in Figure 14.

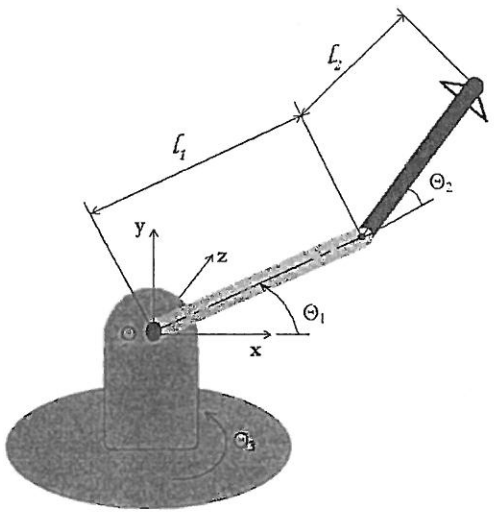

Figure 14 - PHANToM device workspace

The end-effector position (x^u, y^u, z^u) to the joint displacements ($\theta_1{}^u$, $\theta_2{}^u$, $\theta_3{}^u$) in Figure 14 can be written as follows:

$$x(\theta_1^u, \theta_2^u, \theta_3^u) = l_1 \cos\theta_1^u \cos\theta_3^u + l_2 \cos(\theta_1^u + \theta_2^u)\cos\theta_3^u \quad (1)$$

$$y(\theta_1^u, \theta_2^u, \theta_3^u) = l_1 \sin\theta_1^u + l_2 \sin(\theta_1^u + \theta_2^u) \quad (2)$$

$$z(\theta_1^u, \theta_2^u, \theta_3^u) = l_1 \cos\theta_1^u \sin\theta_3^u + l_2 \cos(\theta_1^u + \theta_2^u)\sin\theta_3^u \quad (3)$$

Changing the angles and axes to the PHANToM specified angles and axes that are specified by GHOST Software Development Kit (SDK), the end effector position (x^p, y^p, z^p) to the joint displacements $(\theta_1^p, \theta_2^p, \theta_3^p)$ be written as follows by modifying the above equations:

$$x(\theta_1^p, \theta_2^p, \theta_3^p) = -l_1 \cos\theta_2^p \sin\theta_1^p - l_2 \cos(\theta_3^p - \pi/2)\sin\theta_1^p \quad (4)$$

$$y(\theta_1^p, \theta_2^p, \theta_3^p) = l_1 \sin\theta_2^p + l_2 \sin(\theta_3^p - \pi/2) \quad (5)$$

$$z(\theta_1^p, \theta_2^p, \theta_3^p) = l_1 \cos\theta_2^p \cos\theta_1^p + l_2 \cos(\theta_3^p - \pi/2)\cos\theta_1^p \quad (6)$$

And simplifying the equations:

$$x(\theta_1^p, \theta_2^p, \theta_3^p) = -l_1 \cos\theta_2^p \sin\theta_1^p - l_2 \sin(\theta_3^p)\sin\theta_1^p \quad (7)$$

$$y(\theta_1^p, \theta_2^p, \theta_3^p) = l_1 \sin\theta_2^p - l_2 \cos(\theta_3^p) \quad (8)$$

$$z(\theta_1^p, \theta_2^p, \theta_3^p) = l_1 \cos\theta_2^p \cos\theta_1^p + l_2 \sin(\theta_3^p)\cos\theta_1^p \quad (9)$$

Thus the Jacobian can be written as:

$$J = \begin{bmatrix} -l_1 \cos\theta_2{}^p \cos\theta_1{}^p - l_2 \sin\theta_3{}^p \cos\theta_1{}^p & l_1 \sin\theta_2{}^p \sin\theta_1{}^p & -l_2 \cos\theta_3{}^p \sin\theta_1{}^p \\ 0 & l_1 \cos\theta_2{}^p & l_2 \sin\theta_3{}^p \\ -l_1 \cos\theta_2{}^p \sin\theta_1{}^p - l_2 \sin\theta_3{}^p \sin\theta_1{}^p & -l_1 \sin\theta_2{}^p \cos\theta_1{}^p & l_2 \cos\theta_3{}^p \cos\theta_1{}^p \end{bmatrix} \quad (10)$$

According to Cavusoglu et al (2001), the torque applied to the motors when the device is stationary is:

$$\tau = \begin{bmatrix} 0 \\ \frac{1}{2} g(2l_1 m_a + 2l_5 m_{be} + l_1 m_c) \cos\theta_2{}^p \\ \frac{1}{2} g(l_2 m_a + 2l_3 m_c - 2l_6 m_{df}) \sin\theta_3{}^p \end{bmatrix} \quad (11)$$

The gravity compensation force applied to the device can be found as:

$$F_{GravComp} = -\ (J^T)^{-1} \tau \quad (12)$$

This force is sent to the device at each haptic update to have gravity compensation.

3.2 Manipulators

Two micromanipulators are used in the experiments. One is a manual used for holding the cell. The other manipulator is a motorized manipulator used to control the motion of the cell probing instrument.

3.2.1 MX7600R

The MX7600R is a 4-axis motorized micromanipulator. It also has the Siskiyou Deisgn Instruments,Inc (SDI) MXC-45 pipette holder mounted to an adjustable clamp along the tool axis. The micromanipulator and pipette holder are shown in Figure 15. The MC2000 controller is used to drive the manipulator stage through a closed loop interface between the controller and the motor encoders. The performance specifications of the manipulator are given in Table-1. [Siskiyou Encoded Device User Manual]

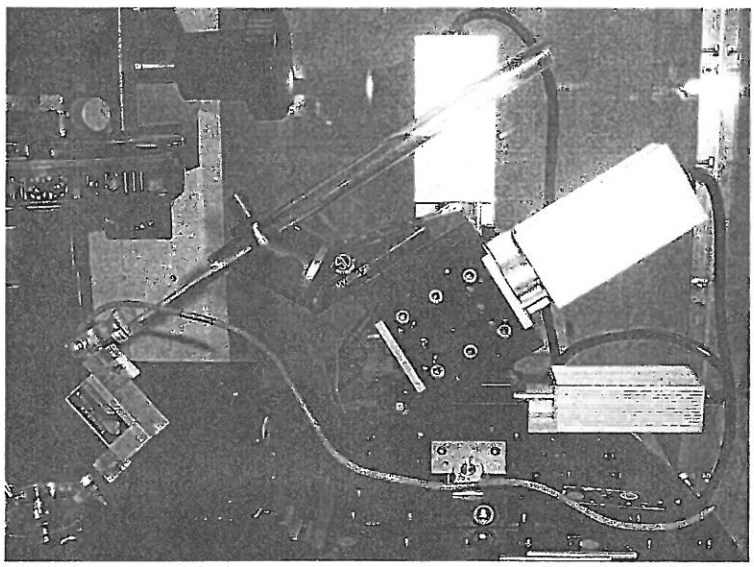

Figure 15 - MX7600R micromanipulator and MXC-45 pipette holder of SDI, Inc.

Table 1 - Performance specifications of M7600R

Maximum Load	2 lbs
Travel / axis	20 mm
Minimum controllable motion	0.1 µm
Backlash	≤ 5 µm
Point to point accuracy	± 2 µm

The manipulator is controlled via the serial port ont eh control PC. The motion of the manipulator can be absolute or relative and the position of the end-effector can be inquired in real time.

3.2.2 Edmund Optics 5-inch Square Linear Translational Stage

The 5-inch Square Linear Translational Stage of Edmund Optics allows low friction linear movement with no backlash or side play. Each stage has one-axis motion, and these two stages are stacked to create two-axis (X-Y) as seen in Each stage has a manual center drive where the straight line accuracy is 2 µm, and position repeatability is 1.2 µm.

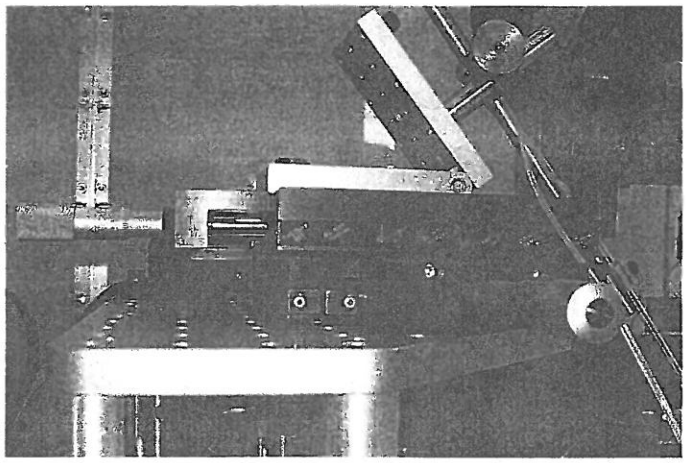

Figure 16 - The 5-inch square linear translational stage of Edmund Optics, Inc.

3.3 Force Sensor

The teleoperation platform is independent of the type of force sensor used, meaning that any kind of force sensor can be used in this platform by using the correct parameters for force calculation at the local site. In this project, GSO-10 load cell of Transducer Techniques, Inc is used in the experiments.

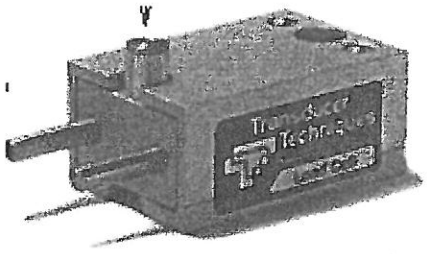

Figure 17 - GSO-10 load cell of Transducer Techniques, Inc.

The GSO-10 load cell has 10 grams of capacity, 10 Volts of maximum voltage output, and deflection of 0.004 inches. It is based on strain gauge bridge. The specifications of the load cell are shown in Table 2 below: [Transducer Technologies Catalog]

Table 2 - Specifications of GSO-10 load cell of Transducer Technologies, Inc

Rated Output (R.O.):	1 mV/V nominal
Nonlinearity:	0.05% of R.O.
Hysteresis:	0.05% of R.O
Nonrepeatability:	0.05% of R.O.
Zero Balance:	1.0% of R.O.
Compensated Temp. Range:	60° to 160°F
Safe Temp. Range:	-65° to 200°F
Temp. Effect on Output:	0.005% of Load/°F
Temp. Effect on Zero:	0.005% of R.O./°F
Terminal Resistance:	350 ohms nominal
Excitation Voltage:	10 VDC
Safe Overload:	150% of R.O.
Deflection Inches:	0.004 @ R.O.
Weight:	1 oz. all ranges

The calibration of the load cell was done by placing 0.25 gram weights on the load stem, measuring the voltage output, and interpolating the points. A linear relationship is found between the force and voltage. The following graph shows the calibration result and the equation in order to convert from voltage to force.

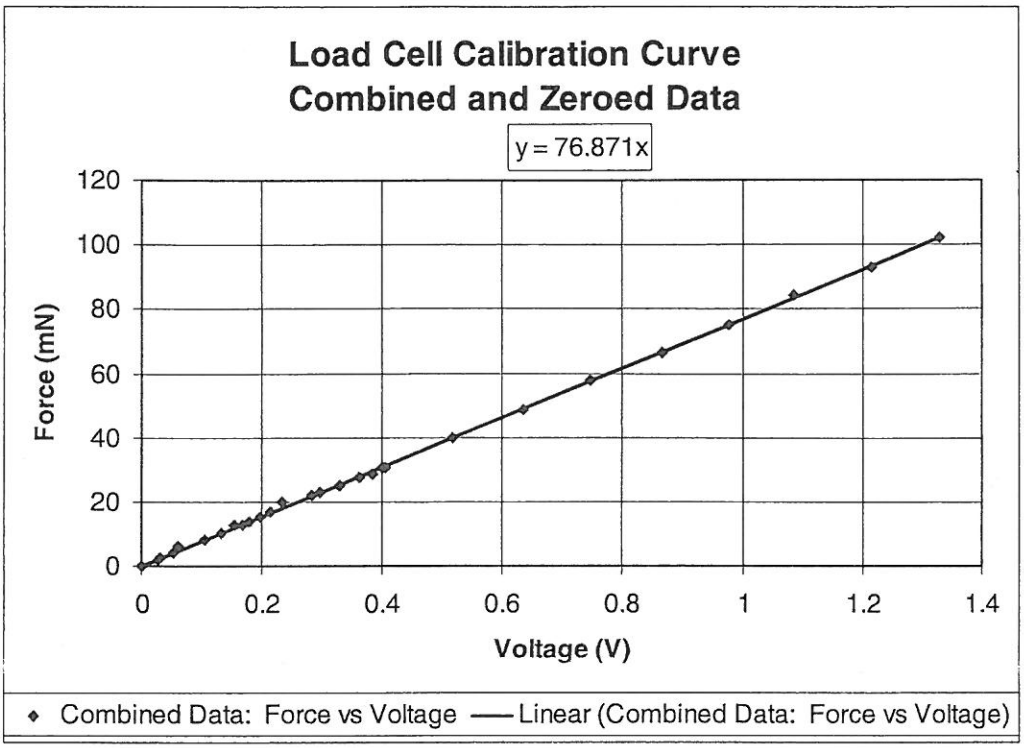

Figure 18 - Calibration curve of the load cell

3.4 Microscope

The Nikon TE2000-U inverted optical microscope is used. The stage of the microscope is motorized with Prior Scientific XYZ stage which can be controlled by the computer. It allows three dimensional motion of the stage: XY plane motion of the base platform and Z axis motion of the objectives. The minimum step size of the stage is 10 μm [Nikon Product Catalog].

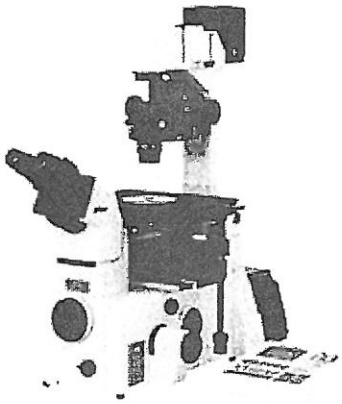

Figure 19 - Nikon TE2000-U

There are 4X, 10X, 20X, and 40X objectives that are used with the microscope. The fields of views with different objectives are shown in Table 3.

Table 3 - Field of views with different objectives

Objective Type	**Field of View (µm)**
4X	2064 X 1548
10X	826 X 619
20X	413 X 310
40X	206 X 155

The CCD camera is mounted to the microscope's port, and it sends 8 bit 640 x 480 pixel images to the computer via frame grabber system. The frame update rate is 30 Hz.

3.5 Teleoperation Platform Software Architecture

The teleoperation platform consists of two main sites, namely local site and remote site which are connected over the internet. There are three applications running in the teleoperation platform. The local site has the PHANToM and server applications running and the remote site has the application controlling the micromanipulator.

3.5.1 Network

Two sites are connected over TCP/IP connection. The server maintains two sites updated in terms of data. The server runs on the local site machine, and both the PHANToM and micromanipulator applications connect to the server and exchange data. The basic flow diagram of the network is shown in Figure 20.

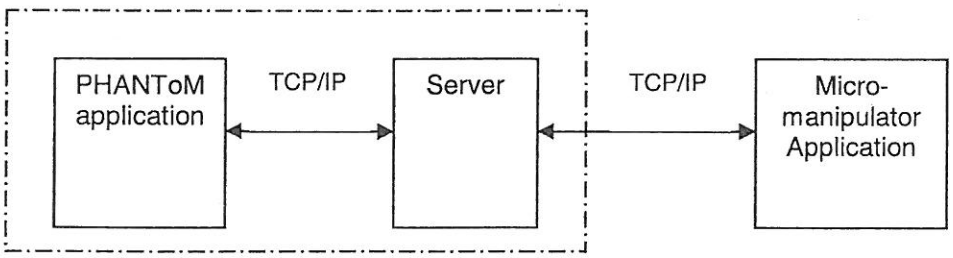

Figure 20 - Basic flow diagram of the network

There are four different communication types; PHANToM to server, server to PHANToM, Micromanipulator (MM) to server, and server to Micromanipulator. The data structures sent over the network for each case is shown in Figure 21.

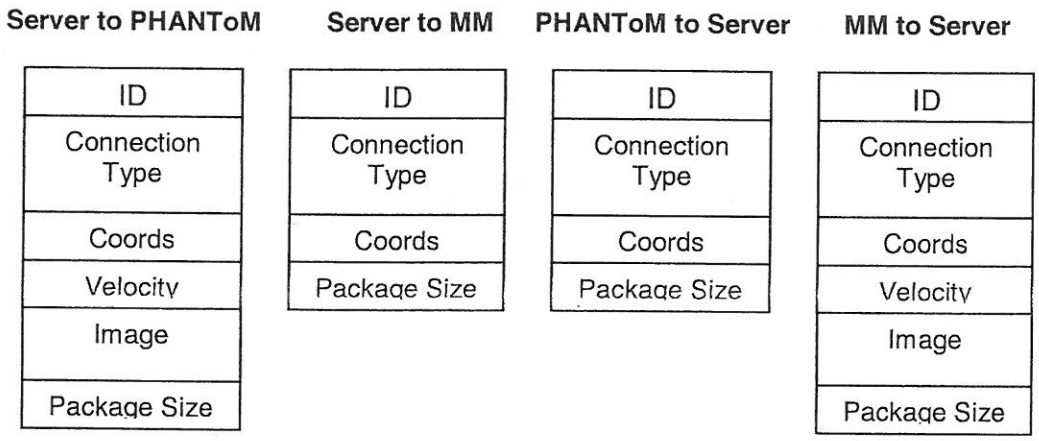

Figure 21 - Data structures sent over the network according to connection

The micromanipulator application sends the 2-D position, velocity, and image frame to the server and receives the 2-D PHANToM position. The PHANToM sends its position, and receives the micromanipulator position, velocity and image.

3.5.2 Local Site

3.5.2.1 Server

As its name implies, the server application helps PHANToM and micromanipulator applications to exchange data. It runs in a loop where at anytime one of the applications can connect, update its data and retrieve the new data.

It is optional to also use the server as an image displayer (i.e. remote site displayer), and it proved to give more efficient results. Since the server runs at the same site as the PHANToM, it is inefficient to send the image frame data to the PHANToM while the server itself can display the image frame received while running as a server. On the other hand, in the case that the server application is moved to another machine or the remote site, PHANToM application has the ability to display the image by itself.

3.5.2.2 PHANToM Application

The PHANToM application is the most complex of all. The PHANToM application is used for controlling the manipulator at the remote site and to give force and image feedback to the user. It reads data from A/D Board, calculates the force being applied at remote site, calculates the gravity compensation force, sends force to the PHANToM, gets PHANToM position, sends and gets data from the

server and displays remote site environment. The image feedback is optional since the server can also display it. The application is written in C++, and it has two loops: One loop for the force feedback and another loop for the network and image. The force feedback loop runs at about 1 KHz rate, where as the other loop runs at about 30 Hz. Even if there are two separate loops in the application, the flowchart below shows it as combined (Figure 22). This has been done to simplify the program flow, decrease the complexity of the flowchart and give a better understanding to the reader.

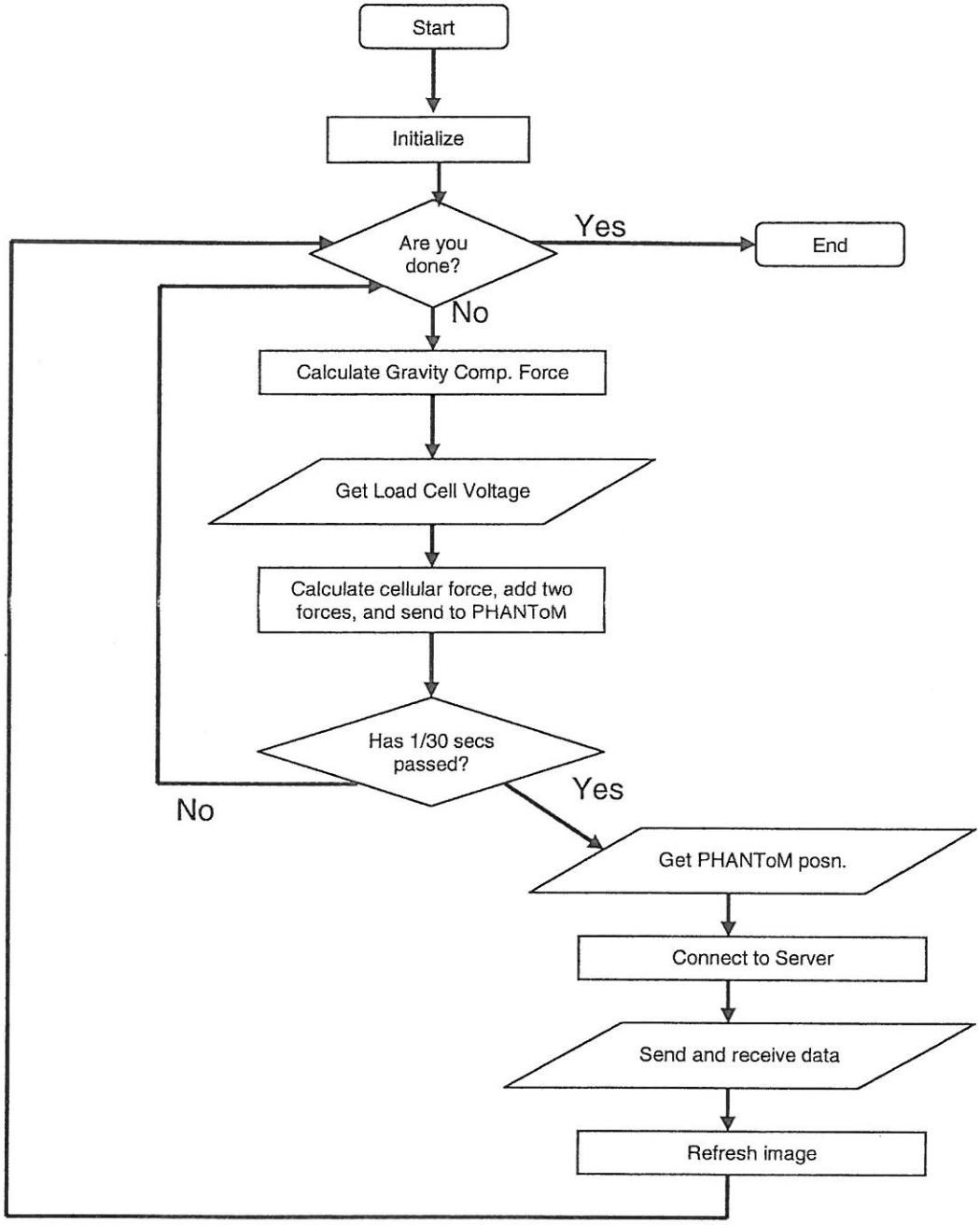

Figure 22 - Flowchart of PHANToM application

3.5.2.2.1 Force Calculation

This application calculates the gravitational force applied at its current position by using the equations given in section 3.1.1, and gives the opposite force to compensate the gravity. The other force sent to the PHANToM is the cellular environment force which is calculated by inputting the load cell voltage to the calibration equation. The orientation of the cell, load cell, and the needle are shown in Figure 23, and the force vector is shown on the right.

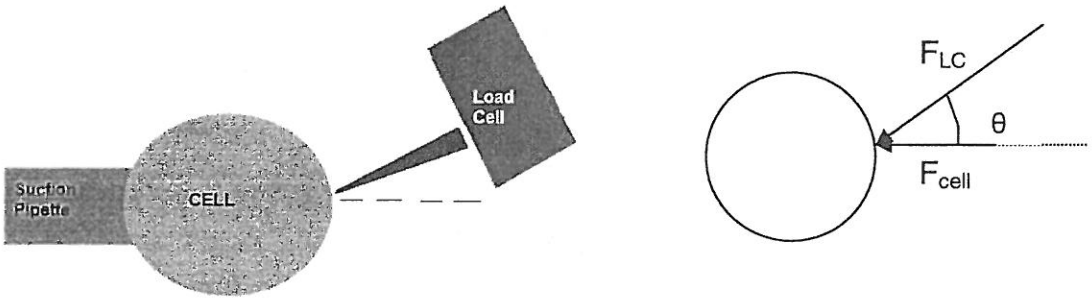

Figure 23 - The orientation of micromanipulation elements, and the force vector.

From the above figure, it is seen that the force applied to the cell and the force applied by the load cell are related as $F_{cell} = F_{LC} * \cos(\theta)$. Since the load cell is not parallel to the ground, the weight of the needle causes the initial voltage (i.e. non-contact voltage) to have a negative offset value. Thus, this initial offset negative voltage is subtracted from all voltage data to shift the initial voltage level to zero.

3.5.2.2.2 Sending and Getting Data from Server

As described in section 3.5.1, The PHANToM application sends position data, and gets image and position data from micromanipulator application. This networking loop works at 30 Hz rate, since the camera mounted on the microscope works at 30 Hz. The PHANToM's GHOST SDK gives ability to program with two different loops; one for haptic update and the other for visual feedback update. The visual feedback update loop is used to connect the server, exchange data, and update the image. Since the PHANToM's and micromanipulator's workspaces are different, there must be a transformation to put them on the same workspace. The transformation method will be explained later in the following section.

3.5.3 Remote Site

The remote site has the microscope, micromanipulators, the cell being manipulated, and other equipment required to control the micromanipulator, acquire the image, and hold the cell.

3.5.3.1 Micromanipulator Application

The micromanipulator application controls all the elements of the remote site and connects with the local site to send and receive data at a rate of 30 Hz. The micromanipulator which controls the needle (or the injection pipette, depending on the operation) is controlled by this application via serial stream port. The position information is translated to the number of counts and fed to the micromanipulator controller to move it to the new position.

The micromanipulator application has two modes: Teleoperation mode and local control mode. In teleoperation mode, the micromanipulator is controlled by the PHANToM at the remote site by necessary translations of workspaces. In local control mode, the micromanipulator is controlled directly by the application. The local control mode gives operator ability to move in X, Y, Z, and tool axes, and in teleoperation mode the operator can move in XY-plane only.

The 640x480 pixel bitmap image acquired by the camera mounted on the microscope is displayed on the application's user interface. The image is also sent to the local site during the teleoperation at a rate of 30 Hz. Each bitmap image takes 300 KB of disk space, thus instead of sending 300 KB at 30 Hz over the internet, the image is compressed and saved in JPEG format and transferred

to the local site. The JPEG image takes about 3KB of disk space which is about hundred times smaller than the bitmap image.

As mentioned before, transformation between the PHANToM and the manipulator workspaces are necessary to perform operation. X-axis movement is more critical than Y-axis, so X-axis movement is taken as the main element of transformation. The transformation is calibrated such that if the operator moves the PHANToM from the zero position (i.e. the position where all three axes of PHANToM workspace are orthogonal to each other) to the maximum position that can be reached in negative x-axis, this distance in the PHANToM workspace will be equal to the movement of the needle from the middle to the leftmost point in x-direction. The corresponding PHANToM distance is 190 mm for this transformation. Using a 4X objective, 31 pixels of the image is equal to 100 μm, since the image is 640 pixels wide, half of it gives 1023 μm as the distance that must be traveled with the transformation. Dividing 1023 μm by 190 mm gives 5.38 μm/mm and the resulting positions of the two sites are related such that:

$$Pos(x, y)_{remote} = Pos(x, y)_{local} * 5.38 \frac{\mu m}{mm}$$

The flowchart of the remote site application is given in Figure 24.

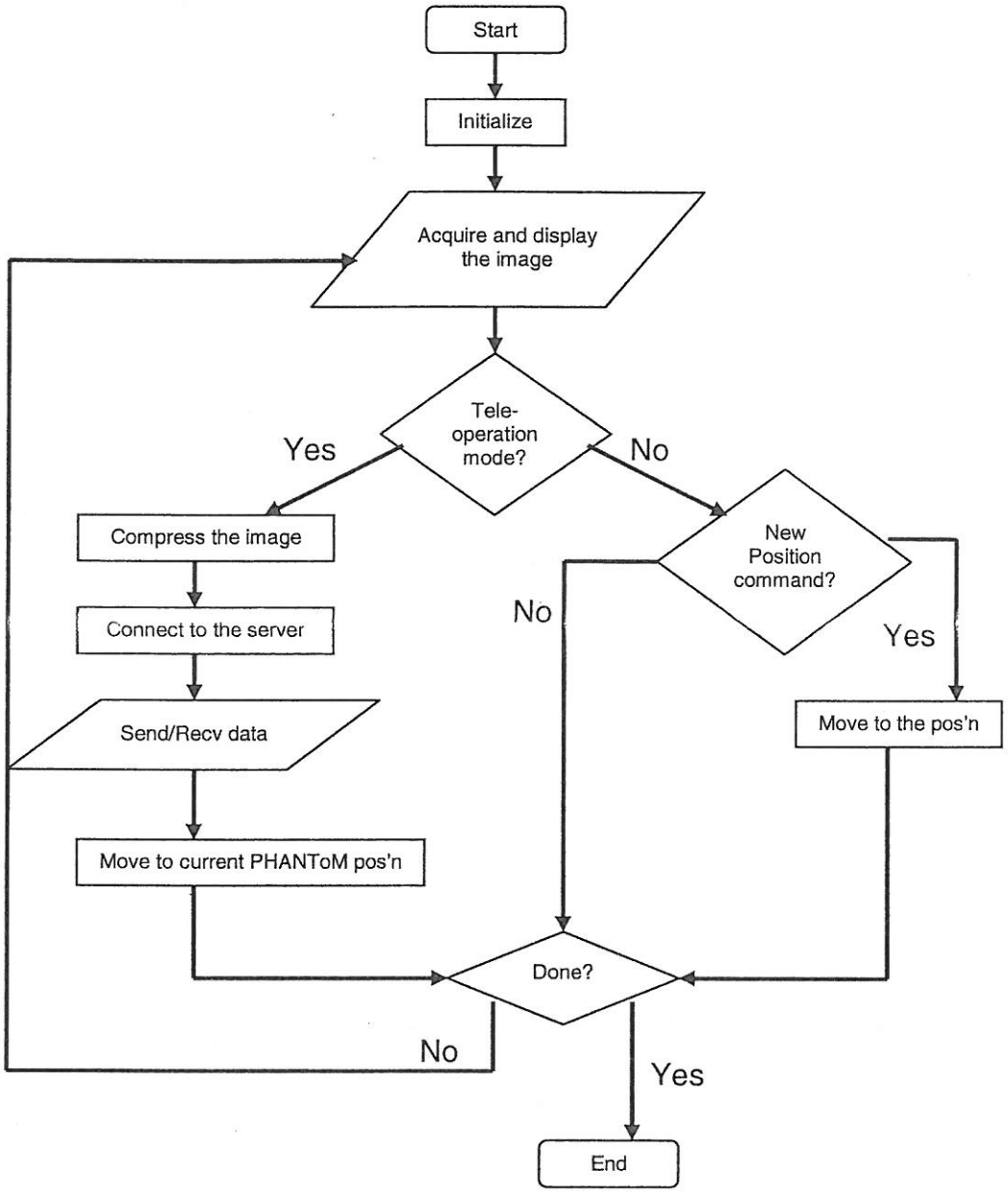

Figure 24 - The Micromanipulator application flowchart

3.6 Experiments

Four set of experiments are done in order to demonstrate the use of the teleoperation platform in manipulation and characterization at micro-scale. The first experiment is a peg-in-the-hole experiment, and the other three set of experiments are done with fish egg cells to represent examples for the characterization and manipulation of single cells.The second experiment which is the initial experiment for the characterization of cells led the idea for the third and fourth experiments.

3.6.1 Microassembly Experiment

3.6.1.1 Purpose

Push the object in the hole by controlling the manipulator with PHANToM.

3.6.1.2 Materials

- Plastic block with dimensions of 0.4 mm X 0.8 mm X 1 mm,
- Plastic fixture with 1mm width groove on one side and a 0.6 mm width of groove at the other.

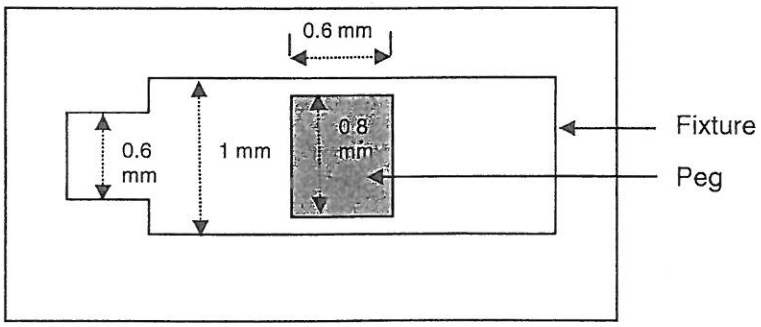

Figure 25 - Peg in the hole experiment materials

3.6.1.3 Methods

i) The plastic fixture is positioned under the microscope.

ii) The plastic object (peg) is placed with 1mm side vertically in the middle of the groove, and the needle for manipulation is positioned next to the peg.

iii) The remote site connects to the local site, and starts to send and get data over network.

iv) The operator at the local site operates the needle with PHANToM, reorientates, and inserts the peg in the hole.

3.6.2 Egg Cell Experiment #1

3.6.2.1 Purpose

The purpose of this experiment is to make indentations of the cell membrane and observe the characteristic responseof the egg cells.

3.6.2.2 Materials

- 4ml of 30% NaCl solution,
- 10 Whitefish egg cells,
- Load cell with 100 μm diameter needle placed on the micromanipulator.

3.6.2.3 Methods

i) Place ten egg cells in the solution and keep them for five minutes.

ii) Select an egg cell, apply suction to hold and position in the field of view of the microscope. Focus the central plane of the cell.

iii) Position the needle to within about 2.5 μm to the cell membrane, in the same focal plane as the cell. Measure the angle of the load cell to the focal plane.

iv) Move the needle with 5 μm steps in the direction of the cell membrane until 500 μm total indentation is achieved. Then move the needle in the opposite direction to the starting position.

v) Repeat step (iv) for 25 μm, 50 μm, 100 μm, 250 μm, and 500 μm steps, indenting all up to 500 μm.

3.6.2.4 Data Interpretation

Data from the load cell which is collected by A/D board is saved and fed to the calibration equation which converts the voltage to the force that is applied to the cell. The equation is as follows:

$$F(t) = (V(t) - V_o) * 76.871 * \cos(\theta),$$

where V_o and θ are the initial voltage of the load cell and angle of the load cell to the focal plane, respectively.

After applying the equation, the chart showing force vs. time is displayed.

3.6.3 Egg Cell Experiment #2

3.6.3.1 Purpose

The relaxation characteristics of the egg cell are studied in these tests. Five cells with different diameters are tested under 5 different indentation levels. This yields a 5x5 matrix of data for analysis.

3.6.3.2 Materials

- 30% NaCl solution,
- Whitefish egg cells,
- Load cell with 100 μm diameter needle placed on the micromanipulator.

3.6.3.3 Methods

i) Place ten egg cells in the solution for twenty minutes.

ii) Select an egg cell with a diameter different than other tested diameters (select randomly if none has been done). Apply suction to hold the cell and position it in the field of view. Focus the central plane of the cell.

iii) Position the needle to within about 2.5 μm to the cell membrane, in the same focal plane as the cell. Measure the angle of the load cell to the focal plane.

iv) Move the needle a single step of 200 μm in the direction of the cell membrane. Wait for 10 minutes and then move the needle in the opposite direction back to the starting position.

v) Repeat above step (iv) for 300 μm, 400 μm, 500 μm, and 600 μm indentation level.

vi) Go to step (i) until 5 egg cells are tested.

3.6.3.4 Data Interpretation

Data from the load cell which is collected by A/D board is saved and fed to the calibration equation explained in Section 3.6.2.4. After applying the equation, the chart showing force vs. time is displayed, and the data is used to characterize and observe the properties of the cell relaxation.

3.6.4 Egg Cell Experiment #3

3.6.4.1 Purpose

Five different cells at five different concentrations of NaCl are tested in order to observe the effects of osmosis and salinity on cell stiffness.

3.6.4.2 Materials

- 4 ml's of 25%, 18.75%, 12.5%, 6.25% and 0% NaCl solutions,
- 20 Whitefish egg cell,
- Load cell with 100 μm diameter needle placed on the micromanipulator.

3.6.4.3 Methods

Five cells are used, and each cell starts at a different concentration level of NaCl and ends at zero concentration. The timeline for the experiment is drawn in Figure 26. Each cell starts with a lower concentration, and goes to lower concentrations until 0% is reached. The squares with a dot in it denote that they are the first osmosis effect observations for the corresponding cells.

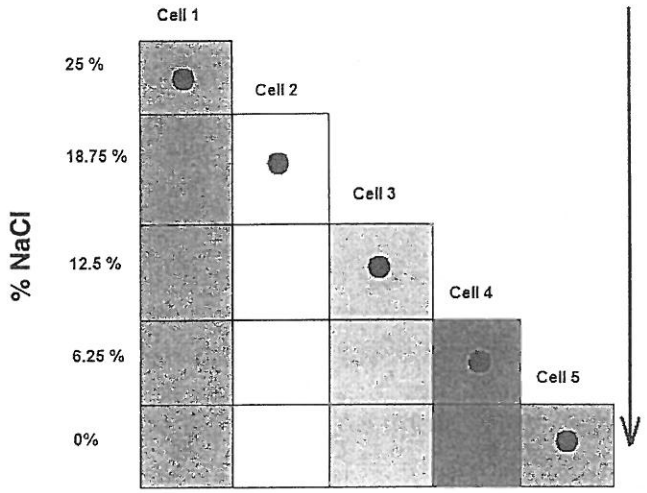

Figure 26 - Experiment setup schematic

The cell handling and manipulation steps are as follows:

i) Fill petri dishes with 4 ml of each solution and number them starting from the highest level as #1and the lowest as #5 which is pure H_20.

ii) Place dish #1 under the microscope, and position the suction pipette and micromanipulator in the field of view.

iii) Choose one egg cell, place it near to the suction pipette. Apply suction to hold the cell, and focus in the central plane of the cell.

iv) Position the needle as close as possible (ideally within 2.5 µm) to the membrane and in the same focal plane with the cell, and set this as home position for the manipulator.

v) Move the needle 25 µm steps in the direction of the cell membrane until 600 µm total indentation is achieved. Then move the needle in the opposite direction to the home position.

vi) Repeat step (iv) through (v) at the second, sixth and eleventh minutes that the cell is in a particular solution.

vii) Repeat steps (ii) through (vi) but with the lower concentration level until petri dish #5 is reached.

viii) Repeat steps (ii) through (vii) but with the next egg cell starting from the petri dish which has the same number as the egg cell (e.g. Cell #3 will start from petri dish #3 and end at petri dish #5).

3.6.4.4 Data Interpretation

Data from the load cell which is collected by A/D board is saved and fed to the calibration equation explained in Section 3.6.2.4. After applying the equation, the chart showing force vs. time is displayed, and the data is used to characterize and observe the effects of NaCl concentration and osmosis on the egg cells.

3.6.5 Force Feedback vs. Non-force Feedback Experiment

3.6.5.1 Purpose

The purpose of this experiment is to test whether the force feedback is a useful addition to the platform or not.

3.6.5.2 Materials

- One Whitefish egg cell

3.6.5.3 Methods

The egg cell will be placed and focused under the microscope. The microneedle will be positioned at a distance of 800 µm to the cell membrane.

The goal is to move the needle until it touches the cell membrane. The operator will try this by using the manual mode and teleoperation mode with force feedback. In the manual mode, the operator enters the displacement on the screen and clicks the button to move the needle until a visual deformation of the cell membrane is observed. In the teleoperation mode, the operator moves until the force is sensed with PHANToM device.

Two points on the cell surface will be determined to touch; one in the north hemisphere and the other in the south hemisphere part of the cell which are about 400 µm above and below the median. After the operator touches one of these points, he has to go back to the starting position and do the same operation for the other point.

3.6.5.4 Data Interpretation

The time duration of the experiment will be recorded for the manual and teleoperation modes which will be compared for analysis.

4. Results and Analysis

4.1 Microassembly Experiment

The sample pictures of the experiment can be seen in Figure 27 below.

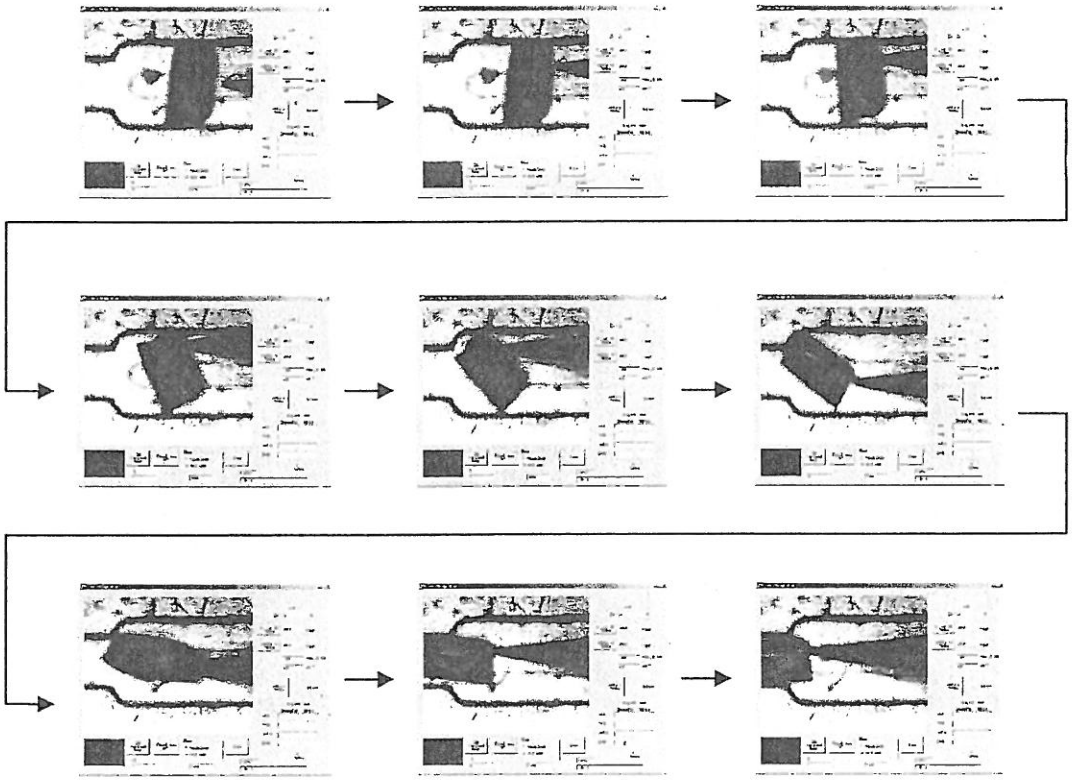

Figure 27 - Peg in the hole experiment

This experiment is completed in 64 seconds in teleoperation mode.

4.2 Egg Cell Experiment #1

As explained in the methods section, the same indentation levels are applied five times for each five cell. One set of results for the Cell #4 of trial #2 is shown in Figure 28 to Figure 33. These figures are representative to all the other results of the 24 sets of data.

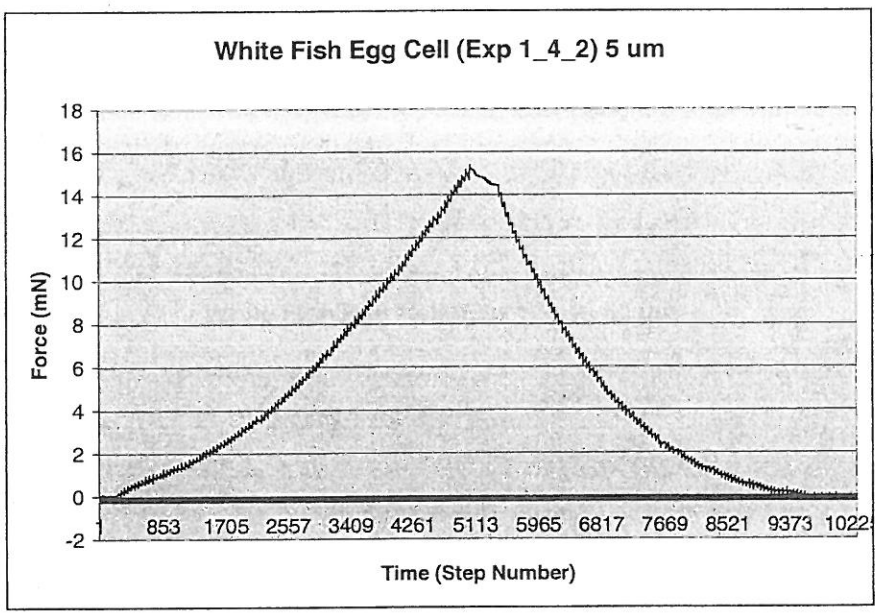

Figure 28 - Experiment 1_4_2: 5 µm steps with 500 µm as the total indentation

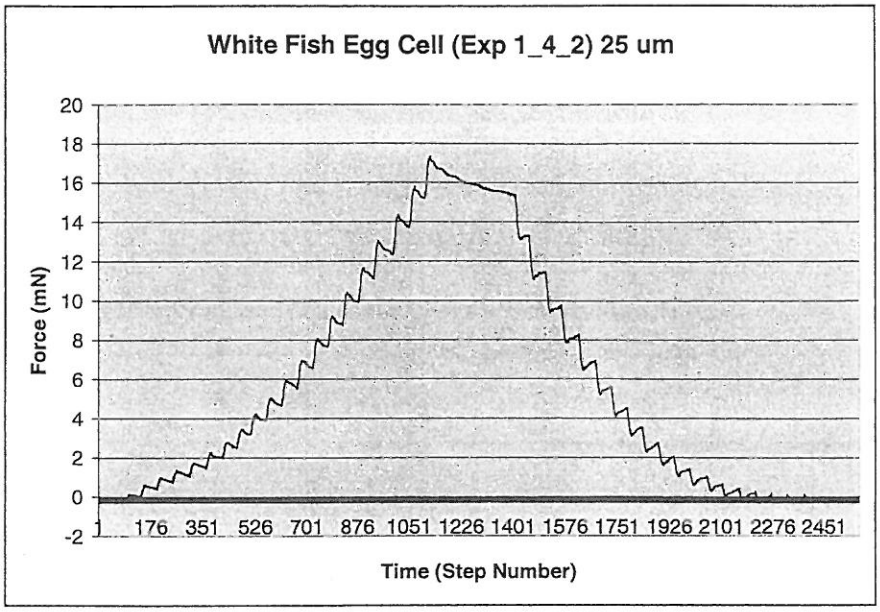

Figure 29 - Experiment 1_4_2: 25 µm steps with 500 µm total indentation

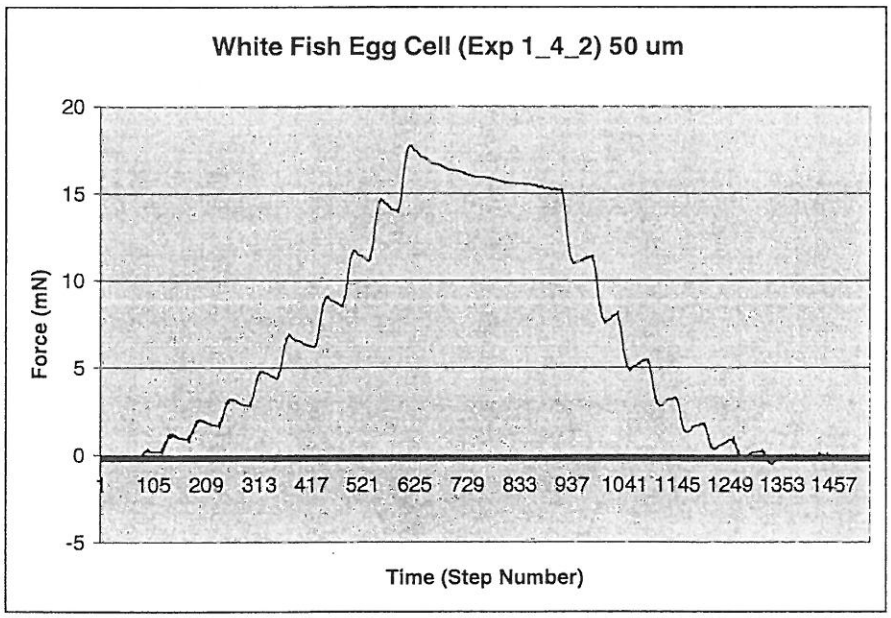

Figure 30 - Experiment 1_4_2: 50 µm steps with 500 µm total indentation

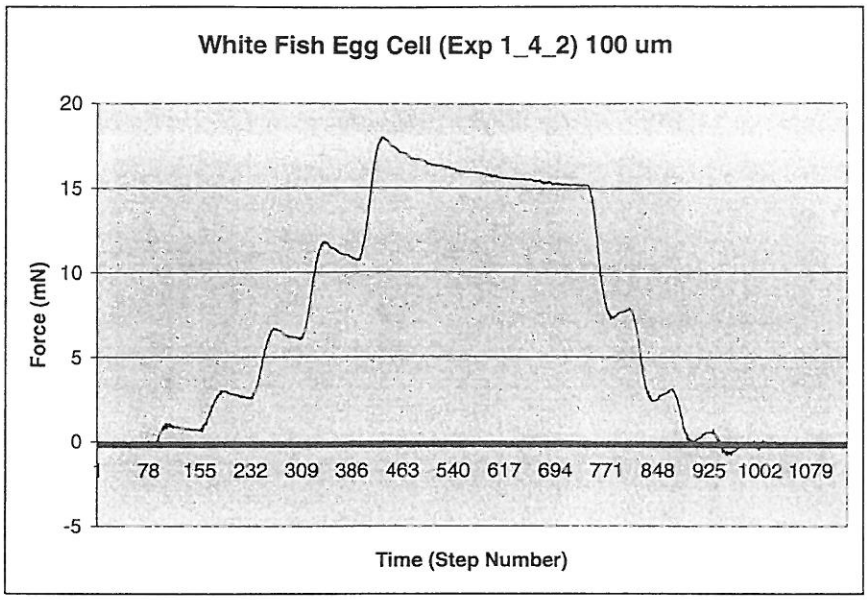

Figure 31 - Experiment 1_4_2: 100 µm steps with 500 µm total indentation

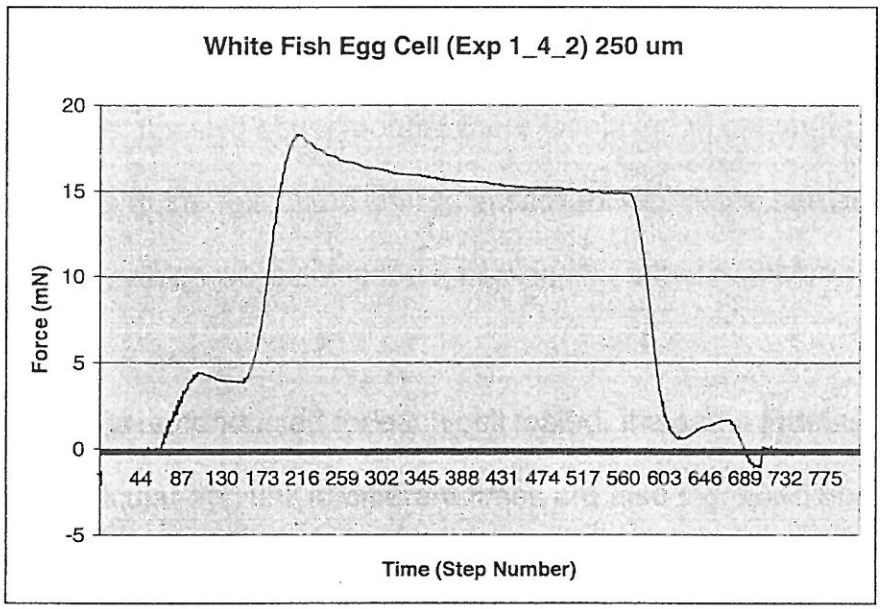

Figure 32 - Experiment 1_4_2: 250 µm steps with 500 µm total indentation

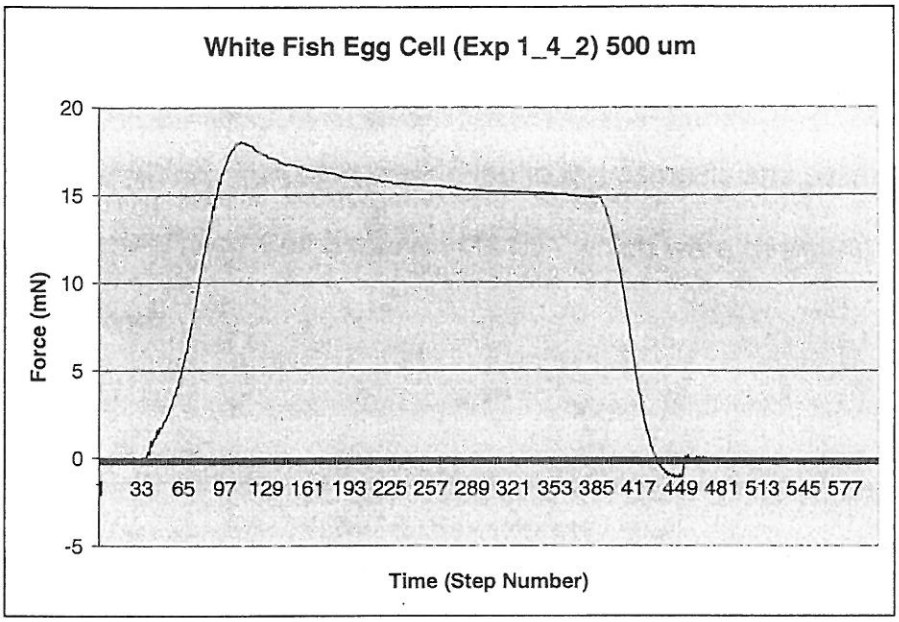

Figure 33 - Experiment 1_4_2: 500 µm steps with 500 µm total indentation

From Figure 28 to Figure 33, the force applied to the cell is about 17 mN at all indentation levels. It's also observed that there is relaxation occurring after each step, which leads to the relaxation characteristics experiments, namely "Egg Cell Experiments #2", which were designed following this experiment type.

Since five trials were conducted for each cell tested, the same indentation step size for that particular egg cell at different times are also extracted from the experimental data. It has been analyzed to observe the effects of time dependency. As an example, 100 µm indentation step size experiments for Cell #3 are analyzed. Figure 34 shows the analysis result for time dependency on the stiffness of the cell. The figure shows the force applied (y-axis) at each 100 µm

step (x-axis), where the maximum indentation is 500 µm (i.e. 5 x 100µm). It was observed that the stiffness of the cell increases with time because of diffusion of the solution into the cell. This observation led to the osmosis and salinity experiments, namely "Egg Cell Experiments #3", which were designed following this experiment type.

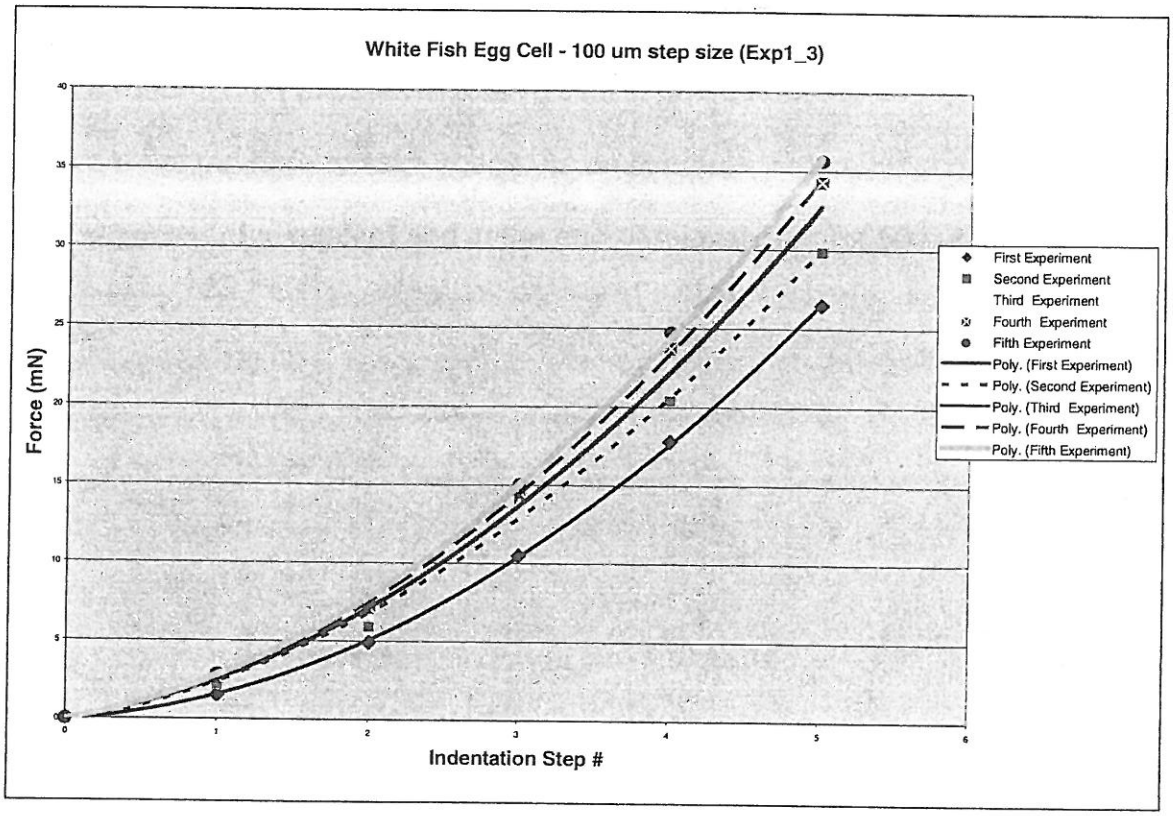

Figure 34 - Experiment 1_3: 100 µm step size experiments for Cell #3

4.3 Egg Cell Experiment #2

As described in the previous section, five different indentation levels of five egg cells with different diameters are tested to see the effects of the diameter on the force and the relaxation characteristic of the cell. Figure 35 shows the initial 600 μm displacement, the relaxation curve for about 10 minutes, and backwards motion of the needle to the home position at the end for Cell #6.[1] All other data obtained for the 24 experiments have similar characteristics as Figure 35 and they are not put here to save space. As an example, Figure 36 shows Cell #4 at the beginning of relaxation and at the end of relaxation for a 500 μm indentation.

[1] 600 μm indentation level experiment data for Cell #3 is corrupted, so an additional experiment is done with Cell #6 in order to complete the experiment set. Thus there are five egg cells used in this experiment set even if cell numbering goes up to Cell #6.

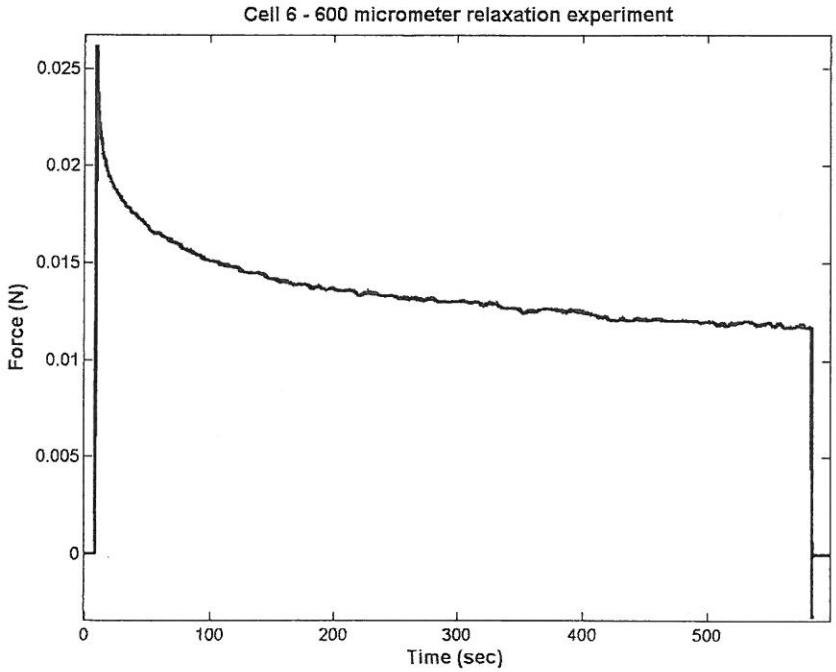

Figure 35 - Experimental data for Cell #6 showing the initial 600 micrometer displacement, the relaxation for about 10 minutes, and backwards motion of the needle to the home position at the end.

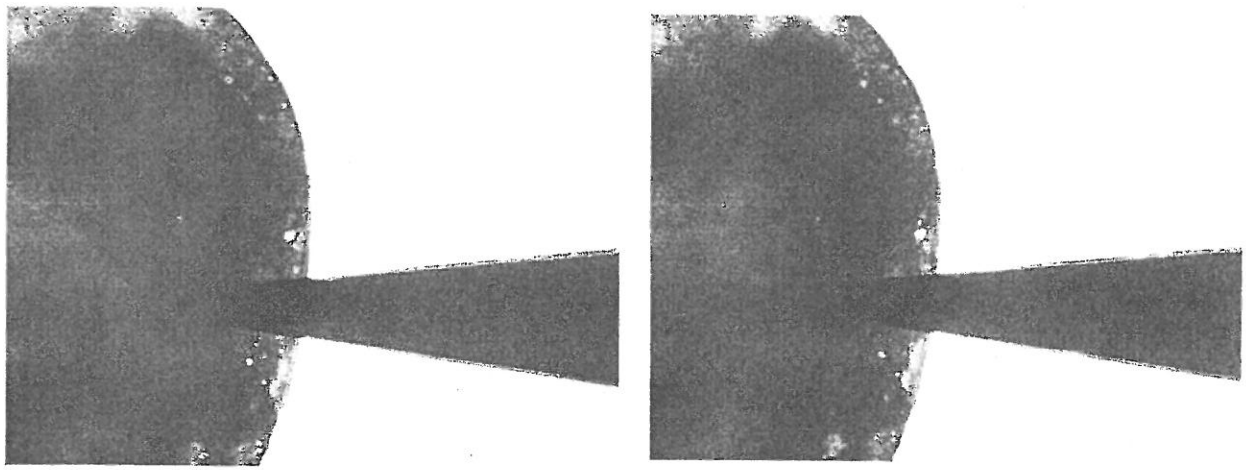

Figure 36 - Cell #4 at the beginning of relaxation and at the end of relaxation for 500 micrometers indentation

4.3.1 Viscoelasticity Characteristics

Relaxation curves are used to model the viscoelastic properties of the cell. The solid linear model (SLM) with an additional parallel spring-damper is used (Figure 37).

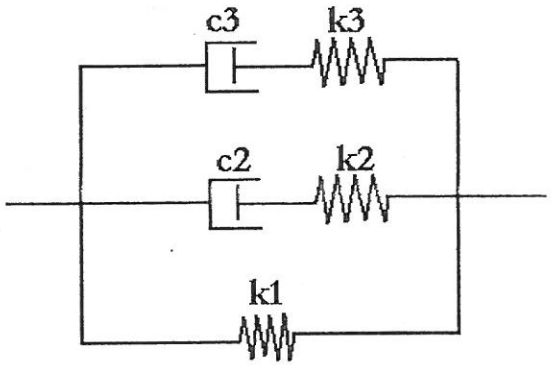

Figure 37 - The model used for analyzing the viscoelasticity of the egg cell

The relaxation of the model of such a system gives the following equation (Appendix A):

$$F(t) = U_0(k_1 + k_2 e^{-\tau_2 t} + k_3 e^{-\tau_3 t})$$

Where U_0 is the initial displacement (indentation level), $k_1, k_2, and\ k_3$ are spring constants, $c_2\ and\ c_3$ are damping constants, and $\tau_2 = k_2 / c_2\ and\ \tau_3 = k_3 / c_3$.

A nonlinear least squares curve fit is applied to the relaxation curve data for each cell and indentation level. The function *nlinfit* of Matlab is used as the software

tool. One set of analysis for Cell #6 is presented in Figure 38 to Figure **42**. The other four analysis plots are similar to the set given here.

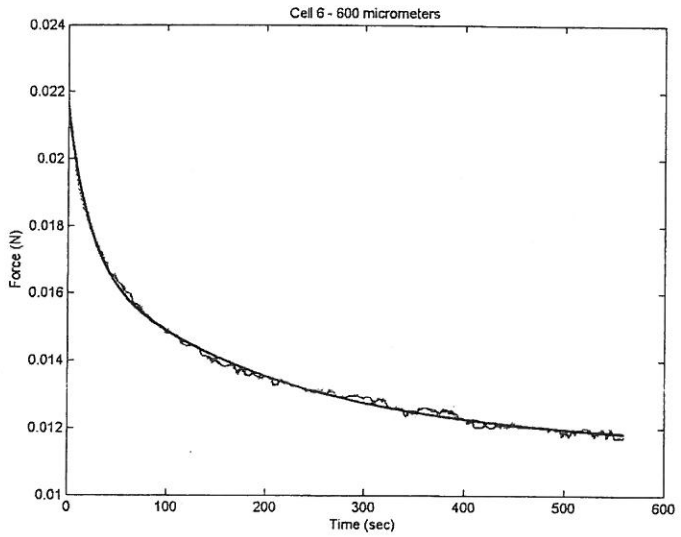

Figure 38 - Relaxation curve with the fit curve - 600 µm indentation

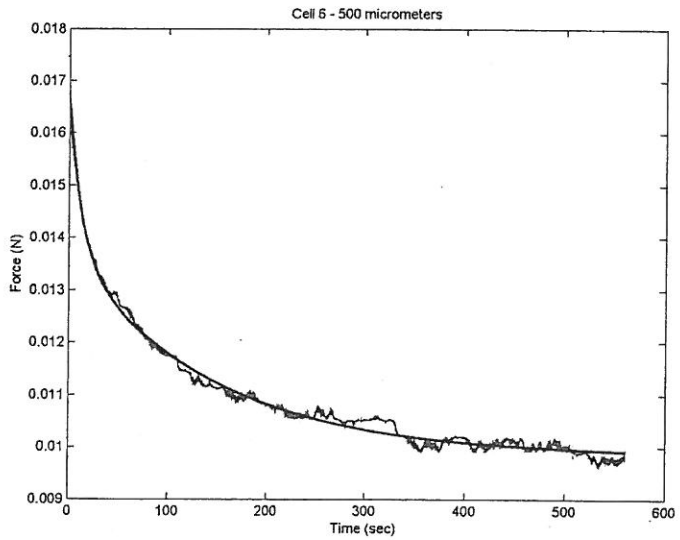

Figure 39 - Relaxation curve with the fit curve - 500 µm indentation

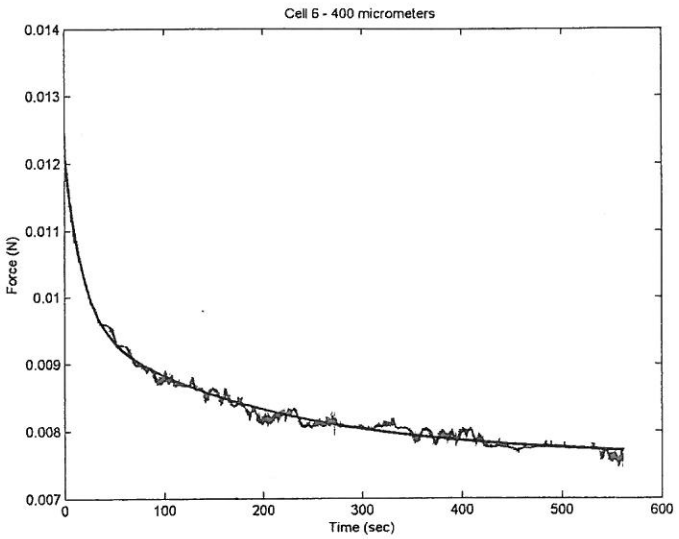

Figure 40 - Relaxation curve with the fit curve - 400 µm indentation

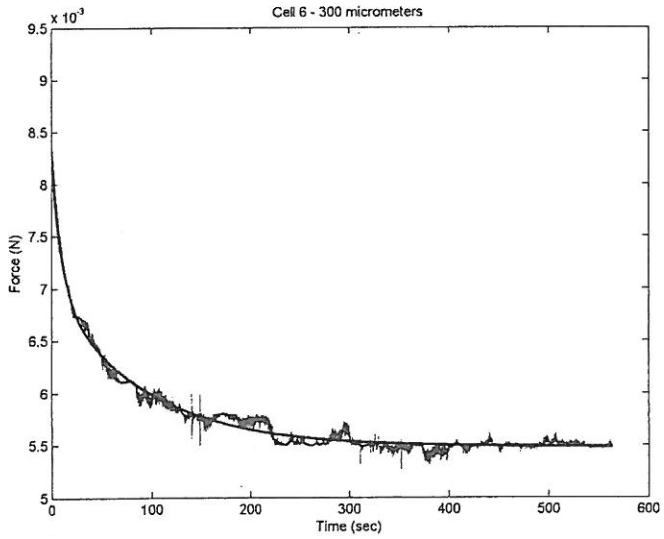

Figure 41 - Relaxation curve with the fit curve - 300 µm indentation

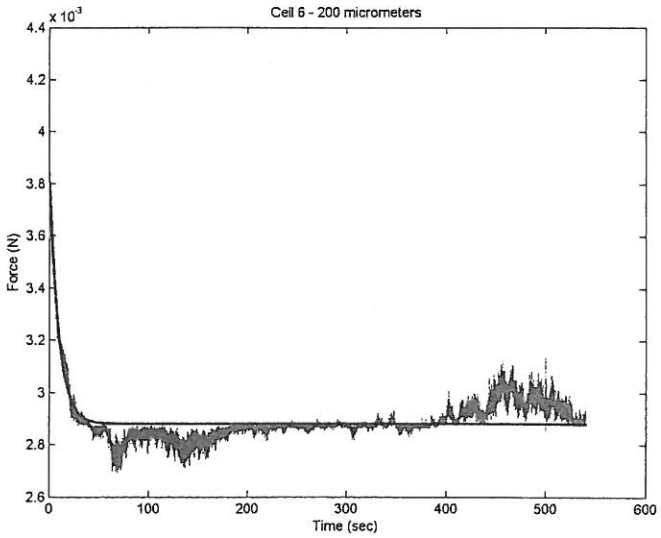

Figure 42 - Relaxation curve with the fit curve – 200 μm indentation

The results for the viscoelasticity analysis are given in Table 4. The columns with gray background color means that the nonlinear least squares function did not converge for the corresponding indentation level. It is observed that 4 out of 6 non-convergent curve fits are at 200 μm indentation level. The force range at 200 μm ranges between 3.9 mN and 2.2 mN.

Table 4 - Cell model fit results

Cell #1 Experiment Results(diameter = 2250 micrometers)

F = U0* (k1 + k2 * exp(-(tau2)*t) + k3 * exp(-(tau3)*t)) ;

Params	600 um	500um	400um	300um	200um
k1	8.0068	7.5041	8.1613	8.1433	7.3928
k2	2.6987	2.7993	2.9204	2.3495	1.4653
c2	30.56285	65.71127	34.47934	31.6218	5.473665
k3	3.7165	3.4699	3.9353	2.7437	2.2412
c3	663.6607	1084.344	771.6275	508.0926	344.8

Cell #2 Experiment Results (diameter = 1935 micrometers)

F = U0* (k1 + k2 * exp(-(tau2)*t) + k3 * exp(-(tau3)*t)) ;

Params	600 um	500um	400um	300um	200um
k1	8.4181	8.225	8.1902	7.733	6.4559
k2	5.7765	4.2207	3.8571	3.8624	2.5873
c2	104.8367	63.27886	45.007	66.13699	23.30901
k3	8.4892	6.1345	6.3271	4.56	3.6248
c3	1438.847	943.7692	832.5132	735.4839	525.3333

Cell #4 Experiment Results (diameter = 2050 micrometers)

F = U0* (k1 + k2 * exp(-(tau2)*t) + k3 * exp(-(tau3)*t)) ;

Params	600 um	500um	400um	300um	200um
k1	15.4814	16.0287	14.5241	13.5979	13.2294
k2	4.7872	3.9811	3.8071	4.1184	2.6991
c2	61.85013	71.99096	51.10201	199.9223	89.07921
k3	9.639	6.8648	5.0089	4.5174	2.1285
c3	2008.125	1346.039	848.9661	4517.4	1252.059

Cell #5 Experiment Results (diameter = 2200 micrometers)

F = U0* (k1 + k2 * exp(-(tau2)*t) + k3 * exp(-(tau3)*t)) ;

Params	600 um	500um	400um	300um	200um
k1	11.5792	11.3836	9.0788	10.3349	9.7346
k2	3.831	3.0344	3.6496	3.1685	2.1615
c2	41.82314	50.74247	104.2743	91.04885	16.96625
k3	7.7636	6.3265	5.9683	4.3594	2.4323
c3	1584.408	1291.122	3141.211	1406.258	1013.458

Cell #6 Experiment Results (diameter = 2100 micrometers)

F = U0* (k1 + k2 * exp(-(tau2)*t) + k3 * exp(-(tau3)*t)) ;

Params	600 um	500um	400um	300um	200um
k1	19.1228	19.6591	18.9847	18.2593	14.3961
k2	7.675	5.8447	6.3424	4.5022	4.4864
c2	164.6996	75.02824	113.6631	42.8781	41.81174
k3	9.1371	7.7481	5.0642	5.0125	0.3197
c3	1864.714	1139.426	992.9804	459.8624	2.979497

4.3.2 Relation between Stiffness and Cell Diameter

The relation between the cell stiffness and its diameter are also analyzed under this experiment set. Five different egg cells with different diameters are tested, and the force applied to the cell membrane is recorded at each indentation level. The results are shown in Table 5.

Table 5 - The force applied at each indentation level for five different egg cell sizes

Cell #	Diameter (µm)	Force at Indentation Level (mN)				
		600 µm	500 µm	400 µm	300 µm	200 µm
2	1935	14.7	9.9	7.8	5.1	2.6
4	2050	18.6	14.2	9.7	7.3	3.9
6	2100	23.1	17.3	12.8	8.6	4
5	2200	14.3	11	8	5.7	2.9
1	2250	9	7.4	6.2	4.1	2.2

4.4 Egg Cell Experiment #3

In this experiment set, time dependency of stiffness is analyzed. The results are given in the following figures (Figure 43 - Figure 47). Each plot title shows a cell number and the experiment number of the related cell separated with a dash (e.g. Cell#2-1 is the first experiment done with Cell #2). The figures start from 100, meaning that the initial force is scaled to 100 and all other forces drawn show the force relative to the initial force. In order to make comparison easier, it

is assumed that the final force of an experiment is the same as the initial force of the the next experiment for the same cell (e.g. the last force measurement of Cell#2-1 is equal the initial force measurement of Cell#2-2).

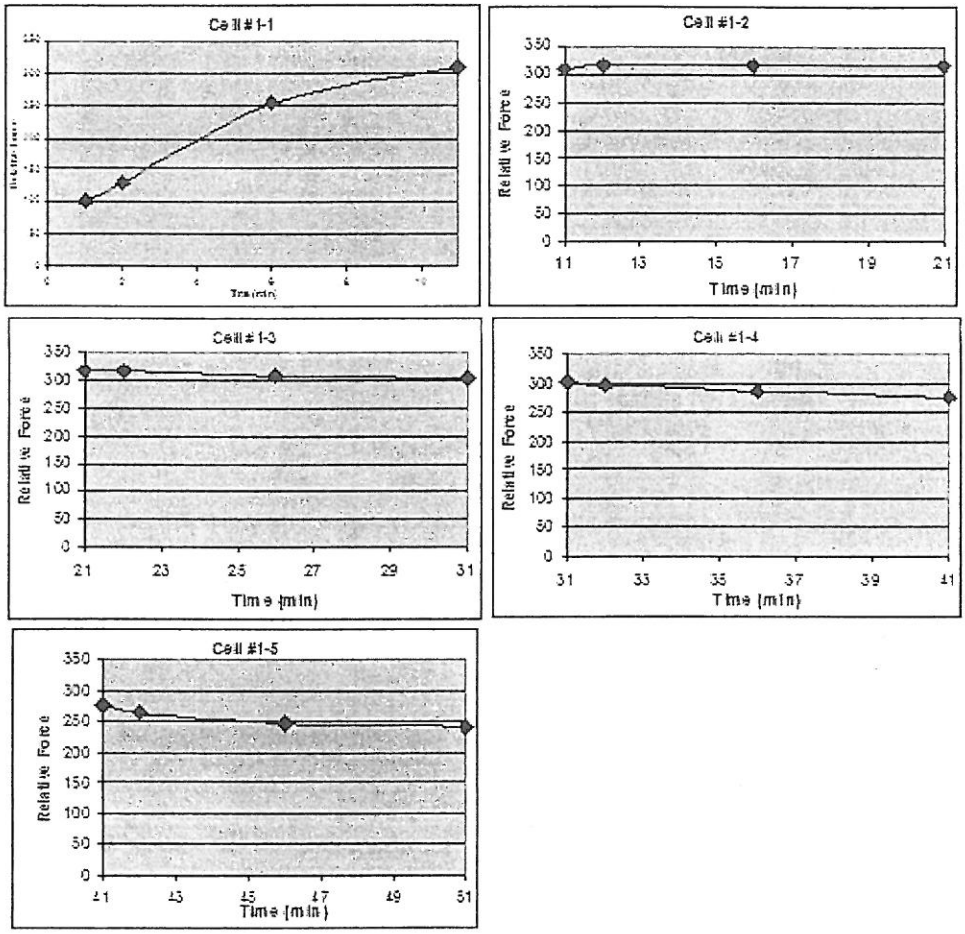

Figure 43 - Experiment results for Cell #1

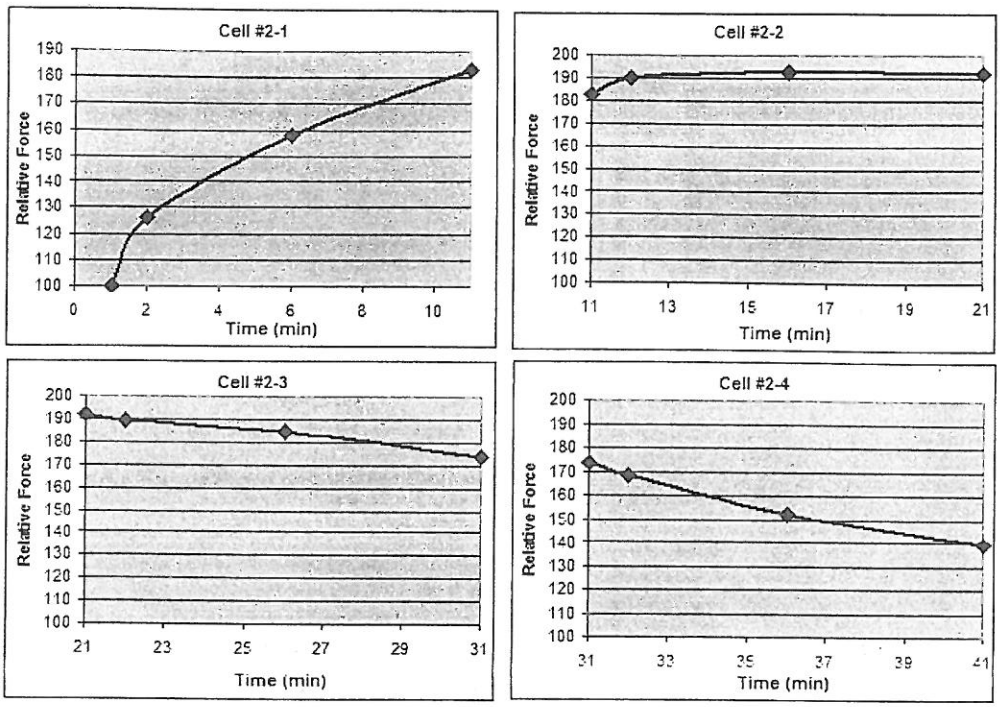

Figure 44 - Experiment results for Cell #2

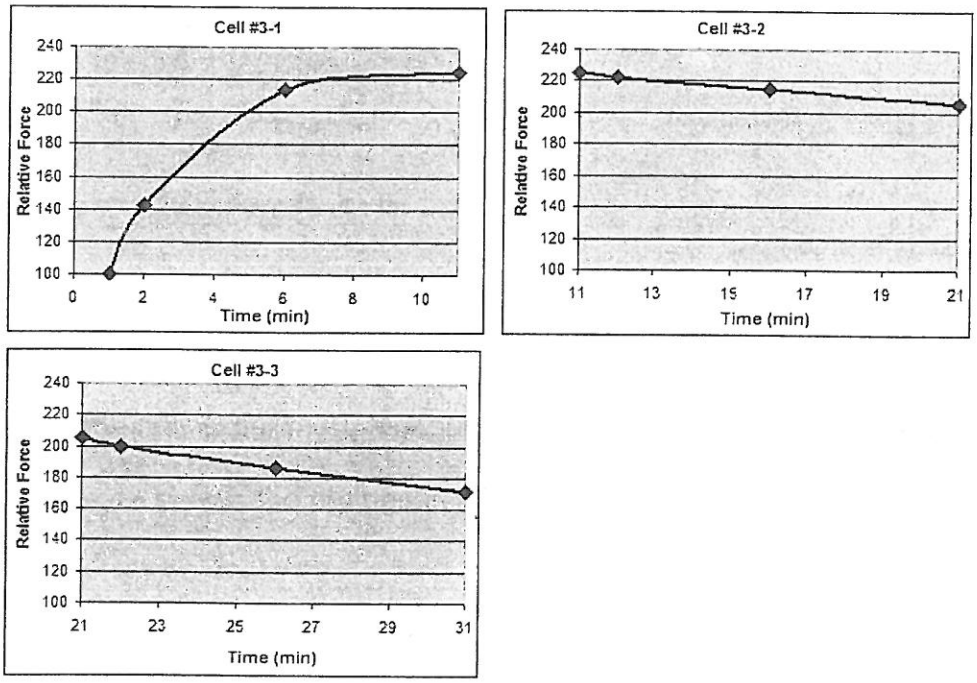

Figure 45 - Experiment results for Cell #3

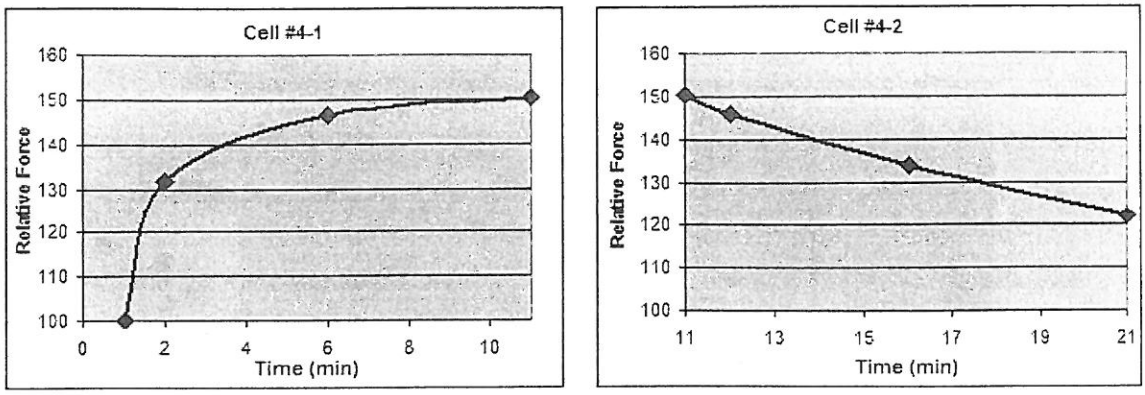

Figure 46 - Experiment results for Cell #4

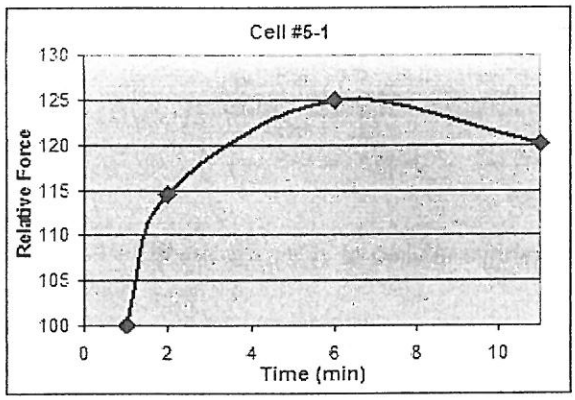

Figure 47 - Experiment results for Cell #5

Further analysis is done to observe the effects of the salinity to the force. Data from the first experiment measurements for each cell is extracted and analyzed. Figure 48 shows the change in force with respect to salinity level.

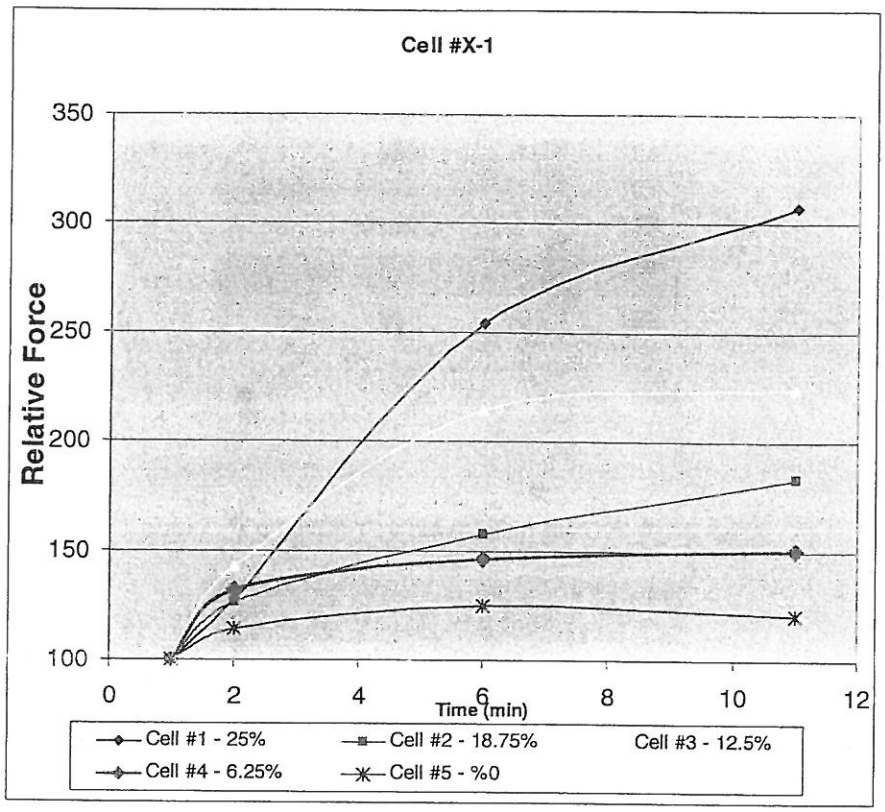

Figure 48 - Effects of salinity to cellular stiffness

4.5 Force Feedback vs. Non-force Feedback Experiment

Table 6 and Table 7 show the results of the 10 trials in manual mode and teleoperation mode, respectively.

Table 6 - Ten experimental trials in manual mode

Trial Number	Time (sec)	Trial Number	Time (sec)
1	198	6	183
2	176	7	191
3	188	8	185
4	188	9	187
5	191	10	182

Table 7 - Ten experimental trials in teleoperation mode

Trial Number	Time (sec)	Trial Number	Time (sec)
1	52	6	45
2	47	7	57
3	51	8	49
4	44	9	47
5	46	10	47

The average operation time for the manual mode is 186.9 sec and it is 48.5 for the teleoperation mode with force feedback.

5. Discussion

The teleoperation platform works by satisfying the required feedback conditions with its 30 Hz image frame rate, 1 kHz force feedback, precise micromanipulator movement, and optimized networking capabilities. The design requirements are also met in this platform by the microassembly experiment where we have hundreds of micrometer dimensions and fish egg cell experiments with around two thousand diameter. The operator was able to feel the force applied to egg cells with smooth force level changes and there was no discrete feeling of the force change. As an example to the overall performance of the teleoperation platform, the object in the microassembly experiment is placed in its target position in 64 seconds over the internet.

The egg cell experiments presented the use of the force sensor and the characteristics of the cells. After the first egg cell experiment, the nonlinearity in the stiffness and time dependency was observed. From these results, second and third egg cell experiments were proposed. The second egg cell experiment was done to compare how the cell stiffness changes by diameter and to see whether it shows viscoelasticity. The model used as the viscoelastic model is shown in Figure 37. There are two dampers in the model and as expected, the nonlinear least squares fitting gave one damping constant 15 to 40 times smaller than the other. This is due to the fast relaxation of the cell at the beginning. There

are five parameters, and the average of the parameters are shown to be 12.3 N/m, 4.2 N /m, 5.9 N/m, 68.9 N.s/m, and 1106 N.s/m for k_1, k_2, k_3, c_1, and c_2, respectively. Since the data didn't converge to nonlinear fit at 200 μm indentation levels except for only one experiment, it may be said that the tested egg cell doesn't show viscoelastic properties at that indentation level or the force sensor doesn't have enough resolution with smaller forces measured at 200 μm.

Another observation from Egg Cell Experiment #2 is that the stiffness of the cell does not depend on the cell diameter. Between five different egg cells with different diameters, the cell with the third biggest diameter showed the maximum stiffness.

The Egg Cell Experiment #3 is done to analyze the effects of salinity to the stiffness and time dependence on salinity of stiffness. The osmosis is observed because of the intracellular environment being denser than the extracellular environment. As the osmosis continued, the volume of the cell increased and change in the stiffness was observed. Initially, the stiffness increased up to a certain time point, and then started to decrease. As a result, the final stiffness of the cell was greater than the initial stiffness. It was observed that for the maximum salinity level of 25% NaCl, the stiffness increased about 3 times, and 1.25 times for the pure H_20 case. The stiffness of the cell reached its peak during osmosis at 22^{nd}, 21^{st}, 11^{th}, 11^{th}, 6^{th} minutes from the maximum to minimum salinity levels, respectively. The relative stiffness increase at the peak was also

related to the salinity level. The maximum relative peak stiffness level was at the maximum salinity level, while the minimum relative peak stiffness level was at the minimum salinity level. During the decrease of the stiffness after the peak, no obvious volume change could be observed, thus the decrease of the stiffness can be explained by the intracellular matrix properties. This shows that it is not only the cell membrane defining the cell stiffness but also intracellular matrix. It can be argued that the cytoskeleton contributes to the cell stiffness with these results. By the time course, the osmosis affects the cytoskeleton and destructs the cytoskeleton structure.

It should be acknowledged that the effects of repeated test on the same egg cell might be a factor on the results and analysis of the experimental data.

The last experiment shows that adding force feedback to the teleoperation platform increased the time efficiency by a huge amount. It is shown that the ratio of the same task in teleoperation with force feedback was 3.85 times faster than in manual mode without force feedback.

6. Conclusion

A teleoperation platform for micromanipulation and characterization of single cell organisms has been developed. Four different sets of experiments with hundreds of individual experiments were implemented to test and show the effectiveness of the platform. A microassembly experiment, namely the peg-in-the-hole, is done to prove the operation of the teleoperation platform. Three egg cell experiments are done to observe the force sensor and micromanipulator capabilities as well as the characteristics of the cell being used with the collected data. Another experiment is designed to see the efficiency of the teleoperation platform with force feedback.

The microassembly experiment was completed in 64 seconds. It is also shown that the egg cell has viscoelastic properties, the cell stiffness has time dependency on osmosis and salinity level, and the stiffness does not depend on the cell diameter.

Human egg cell diameters are about 100 μm and in order to manipulate them in this platform, more improvement must be done in the force sensor and the manual micromanipulator must be changed with a manipulator having a higher resolution so that the cell can be positioned in a more accurate and controllable

way. Also, a suction pipette and a microneedle with smaller diameters are necessary to hold and manipulate the cell.

Another type of force sensor can be used to have smaller resolution such as PVDF based force sensors having sub-microNewton resolution [Fung et al., 2002]. A totally different approach can be to implement a vision based force sensing device.

The platform can also be used in microassembly operations if the necessary tips or accessories are mounted to the micromanipulators. There can be additions to the force reflected to the operator, such as slowing down or blocking the operator if he tries to move the PHANToM arm faster than the micromanipulator can move. This force can be a simple spring-damper force or any other kind of force type depending on the application.

This teleoperation platform was used for the micromanipulation of white fish egg cells which have about 2000 μm of diameter as an example application. By the improvement in the platform, it can perform manipulation in smaller ranges or with higher force resolution. The teleoperation platform, with the presented and discussed experiments, showed satisfactory performance and results and is open for further improvements.

List of References

Abdelwahab MS. Active and Passive Control of Mechanical Vibrations of Cantilevered Beam. MSc, MTC, Cairo, Egypt. October 2002.

Adachi Y, Kumano T, Ogino K. Intermediate representation for stiff virtual objects. Proc. IEEE Virtual Reality Annual Intl. Symposium 1995; 203-210.

Ando N, Korondi P, Hashimoto H. Development of micromanipulator and haptic interface for networked micromanipulation. IEEE/ASME Trans. On Mechatronics. 2001; 6; 4: 417-427.

Arai F, Ando D, Fukuda T. Micro manipulation based on micro physics: Strategy based on attractive force reduction and stress measurement. Proc. IEEE Int. Conf. Robotics and Automation 1995; 236–241.

Ashkin A. Acceleration and trapping of particles by radiation pressure. Physical Review Letters. 1970; 24; 4: 156-159.

Bruican TN, Smyth MJ, Crissnian HA, Salzman GC, et al. Automated single-cell manipulation and sorting by light trapping. Applied Optics. 1987; 26; 24: 5311-5316.

Cavusoglu MC, Feygin D. Kinematics and dynamics of PHANToM(TM) model 1.5 haptic interface. University of California at Berkeley, Electronics Research Laboratory memo M01/15. 2001

Conia J, Edwards BS, Voelkel S. The micro-robotic laboratory: optical trapping and scissing for the biologist. Journal of Clinical Laboratory Analysis. 1997; 11; 1: 28- 38.

Davidson LA, Oster GF, Keller RE, Koehl MA. Measurements of mechanical properties of the blastula wall reveal which hypothesized mechanisms of primary invagination are physically plausible in the sea urchin Strongylocentrotus purpuratus. Dev. Biol. 1999; 209: 221–238.

Fung CKM, Elhajj I, Li WJ, Xi N. A 2-D PVFD force sensing system for micromanipulation and micro-assembly. Proc. of IEEE Int. Conf. of Robotics and Automation. 2002:1489–1494.

Gerovichev O, Marayong P, Okamura A. The effect of visual and haptic feedback on manual and teleoperated needle insertion. Proceedings of Medical Image Computing and Computer-Assisted Intervention (MICCAI), Tokyo, Japan 2002; 147–154.

Ghost SDK Programmer's Guide Version 4.0, SenseAble Technologies Inc. 2002

Kapoor A, Kumar R, Taylor RH. Simple biomanipulation tasks with steady hand cooperative manipulator. Lecture Notes in Computer Science. Springer-Verlag GmbH. October 2003; 141-148.

Kimura Y, Yanagimachi R. Intracytoplasmic sperm injection in the mouse. Biol. Reprod. 1995;52: 709–720.

Lakes R. Viscoelastic Solids. CRC Press, Boca Raton. 1998.

Nikon Product Catalog. http://www.nikonusa.com/template.php?cat=5.

Park J, Jung SH, Kim YH, et al. Design and fabrication of an integrated cell processor for single embryo cell manipulation. Lab Chip 2005; 5: 91-96.

PHANToM Product Catalog. http://www.sensable.com.

Pillarisetti A, Anjum W, Desai JP, Friedman G, Brooks AD. Force feedback interface for cell injection. First Joint EuroHaptics Conference and Symposium on

Haptic Interfaces for Virtual Environment and Teleoperator Systems. 2005: 391-400.

Sheridan TB. Telerobotics, Automation, and supervisory control. MIT Press, Cambridge, Mass., 1992.

Siskiyou Encoded Device User Manual. http://www.sd-instruments.com.

Sun Y, Nelson B. Microrobotic cell injection. Proc. of IEEE Int. Conf. on Robotics and Automation. 2001; 620-625.

Sun Y, Wan KT, Nelson BJ, Bischof J, Roberts K. Mechanical property characterization of the mouse zona pellucida. IEEE Transactions on NanoBioScience. 2003; 2; 4: 279–286.

Tanikawa T, Arai T. Development of a micro-manipulation system having a two-fingered micro-hand. IEEE Transactions on Robotics and Automation. 1999; 15; 1: 152-162.

Transducer Tech Catalog. http://www.transducertechniques.com/load-cells-force-sensors.cfm

Wright WH, Sonek GJ, Tadir Y, Bems MW. Laser trapping in cell biology. IEEE Journal of Quantum Electronics. 1990; 26 ;12: 2148-2157.

Appendix A

The standard linear model (SLM) has a spring element in parallel with a series spring and dashpot (Figure 49).

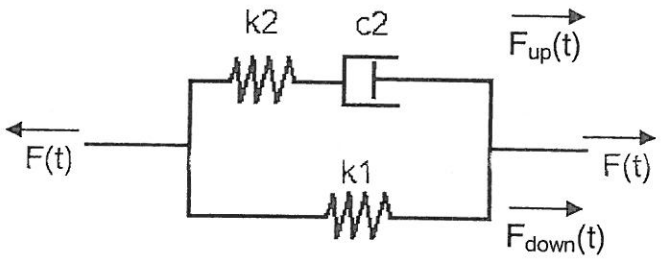

Figure 49 - Standard linear model schematic

The force F(t) applied to the ends of the SLM are equal. F(t) is equal to the addition of force applied to the parallel links. For $F_{down}(t)$, the force and its derivative are as follows:

$$F_{down}(t) = k_1.u(t) \qquad (A.1)$$

$$\frac{d\,F_{down}(t)}{dt} = k_1.\frac{du(t)}{dt} \qquad (A.2)$$

For $F_{up}(t)$, the equation is as follows:

$$\frac{du(t)}{dt} = \frac{1}{k_2}\frac{dF_{up}(t)}{dt} + \frac{1}{c_2}F_{up}(t) \qquad (A.3)$$

$$\Rightarrow k_2\frac{du(t)}{dt} = \frac{dF_{up}(t)}{dt} + \frac{k_2}{c_2}F_{up} \qquad (A.4)$$

Summing equations A.2 and A.4:

$$(k_1 + k_2)\frac{du(t)}{dt} = \frac{d\left(F_{up}(t) + F_{down}(t)\right)}{dt} + \frac{k_2}{c_2}F_{up}(t) \qquad (A.5)$$

$$\Rightarrow (k_1 + k_2)\frac{du(t)}{dt} = \frac{dF(t)}{dt} + \frac{k_2}{c_2}F_{up}(t) \qquad (A.6)$$

In order to eliminate $F_{up}(t)$ from the equation A.6, $F_{down}(t)$ with k_2/c_2 as a coefficient is added to both sides which gives the final equation as follows:

$$(k_1 + k_2)\frac{du(t)}{dt} + \frac{k_2}{c_2}F_{down}(t) = \frac{dF(t)}{dt} + \frac{k_2}{c_2}F_{up}(t) + \frac{k_2}{c_2}F_{down}(t) \qquad (A.7)$$

$$(k_1 + k_2)\frac{du(t)}{dt} + \frac{k_2 k_1}{c_2}u(t) = \frac{dF(t)}{dt} + \frac{k_2}{c_2}F(t) \qquad (A.8)$$

If u(t) is constant (i.e. constant indentation), the relaxation function for this SLM model will be as follows:

$$u(t) = U_0$$

$$\Rightarrow F(t) = U_0\left(k_1 + k_2 e^{-\frac{k_2}{c_2}t}\right) \qquad (A.9)$$

The model used in the analysis of egg cells is an extension of SLM where an additional parallel spring and dashpot is added to the SLM (Figure 37). The addition of another parallel spring and dashpot caused another exponential in the relaxation function showed in equation A.9, and this additional exponential is used to catch the initial fast decrease in the relaxation.

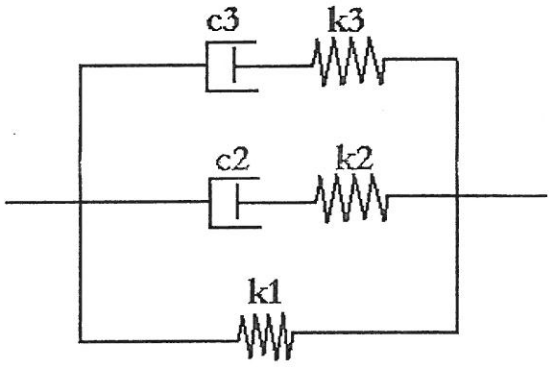

Figure 50 - The model used for analyzing the viscoelasticity of the egg cell

The relaxation function is as follows:

$$u(t) = U_0$$

$$\Rightarrow F(t) = U_0 \left(k_1 + k_2 e^{-\frac{k_2}{c_2} t} + k_3 e^{-\frac{k_3}{c_3} t} \right) \qquad (A.10)$$

For more details on viscoelasticity theory, the reader is referred to Lakes (1998) and Abdelwahab (2002).